Numerical analysis of small scale axial and radial turbines for solar powered Brayton cycle application

Daabo, Ahmed; Mahmoud, Saad; Al-Dadah, Raya; Al Jubori, Ayad; Bhar Ennil, Ali

DOI:
10.1016/j.applthermaleng.2017.03.125

Document Version
Peer reviewed version

Citation for published version (Harvard):
Daabo, AM, Mahmoud, S, Al-dadah, RK, Al Jubori, AM & Bhar Ennil, A 2017, 'Numerical analysis of small scale axial and radial turbines for solar powered Brayton cycle application', Applied Thermal Engineering, vol. 120, pp. 672-693. https://doi.org/10.1016/j.applthermaleng.2017.03.125

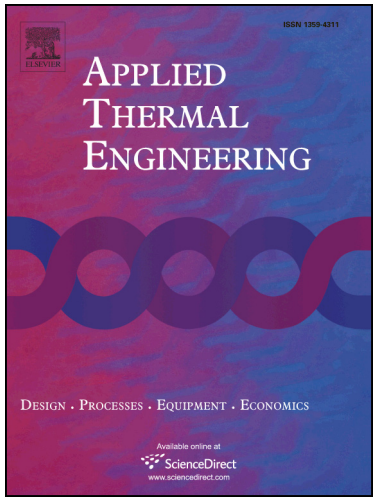

Numerical Analysis of Small Scale Axial and Radial Turbines for Solar Powered Brayton Cycle Application

Ahmed M. Daabo, Saad Mahmoud, Raya K. Al-Dadah, Ayad Al Jubori, Ali Bhar Ennil

PII: S1359-4311(17)32054-9
DOI: http://dx.doi.org/10.1016/j.applthermaleng.2017.03.125
Reference: ATE 10129

To appear in: *Applied Thermal Engineering*

Received Date: 13 July 2016
Revised Date: 10 March 2017
Accepted Date: 28 March 2017

Please cite this article as: A.M. Daabo, S. Mahmoud, R.K. Al-Dadah, A. Al Jubori, A. Bhar Ennil, Numerical Analysis of Small Scale Axial and Radial Turbines for Solar Powered Brayton Cycle Application, *Applied Thermal Engineering* (2017), doi: http://dx.doi.org/10.1016/j.applthermaleng.2017.03.125

Numerical Analysis of Small Scale Axial and Radial Turbines for Solar Powered Brayton Cycle Application

Ahmed M. Daabo[a,b]*, Saad Mahmoud[a], Raya K. Al-Dadah[a], Ayad Al Jubori[a,c], Ali Bhar Ennil[a]
[a] The University of Birmingham, School of Engineering,
Edgbaston, Birmingham, B15-2TT, UK
*Email: axd434@bham.ac.uk, ahmeddaboo@yahoo.com
[b] The University of Mosul, Mechanical Engineering Department, Ninawa, Iraq
[c] University of Technology, Baghdad, Iraq

Abstract

In the current work two types of turbines, axial and radial turbine, with their three configurations, Single Stage Axial, Dual Stage Axial and Single Stage Radial turbines, for solar Brayton cycle applications have been parametrically investigated with the aim of figuring out their performance in terms of efficiency and power output. The mean line design for each turbine was effectively completed in order to figure out the initial guess for the dimensions, the power output and the efficiency. Consequently, the Computational Fluid Dimension CFD analysis was employed for the sake of visualising the 3-Dimentions behaviour of the fluid inside the turbine as well as determining the main output like the power output and the efficiency at different boundary conditions. These boundary conditions were selected to be compatible with a small scale solar powered Brayton cycle. An evaluation for some types of losses such as tip clearance and trailing edge losses as well as the total loss coefficient of the rotor of each configuration, in terms of pressure losses, has been established as well. The current paper deals with Small Scale Turbines SST ranged from 5 to 50 kW as a power output. The outcomes showed that the Dual stage axial turbine performances better at the off design conditions. By contrast, the single stage radial turbine achieved higher power output during the same operating conditions. The results of the CFD analysis have been successfully validated against the experimental work done by the researchers for small scale (axial) compressed air turbine in the lab.

Keywords: 1D& 3D analysis, Single stage and dual stages, Axial turbine, Radial turbine, Brayton cycle.

1- Introduction

In spite of the ease of use technical solutions, about1.3 billion people are still suffering from the lack of having any form of electricity and around 3 billion people are still using open fires for cooking. In spite of the fact that renewable energy is considered one of the main solutions because it is cheap, available, sustainable and environmentally friendly, solar radiation which hits our earth's surface is still not successfully harnessed. Recently, this type of energy is getting more attention by researches, designers and provides companies. As researchers, many papers that include in details different techniques and methods on how to achieve maximum advantages from the solar energy have been published. The considerable benefits from renewable energy and the accelerated importance of its role cannot be denied. As stated by Makower et al [1], that about $51 billion and $52 billion was spent, as an investment, by each China and the USA only in 2011 in spite of the world economic crisis. Moreover, by 2026, it is expected to have about 26% from the overall electricity consumed in the worldwide comes from the renewable energy while it was only around 13% in 2012 [2]. One of the main methods to benefit from the renewable energy is to use it in some power cycles such as Brayton, Rankine and even in the hybrid cycles which have been recently used in different scales. Because of its relative low maintenance and initial cost and simple construction, Small Scale Turbines

SST has become one of the promising technologies. It is commonly accepted that the power output is the factor used when it is needed to classify the turbines scales, so, this scale is from 5 – 500kW or below 200 kW [3, 4] respectively.

Some papers on the cycle's analysis and optimization have been published as those in [5, 6]. However, there was nothing in the mentioned researches regarding the turbines' role. Other components of the cycle such as the thermal receiver have been intensively studied and recently published [7-9]. Even though some studies on the cycle analysis did investigate and considered the turbine such as those in [10, 11], however, they have deal with different scale, large scale. One of the main reasons for carrying out the current study is the unavailability, from the published studies, that investigate in depth the performance in both; on design and off design conditions with this range of turbine power outputs. In current study a comparison, with a range of around 5 to 45 kW for small scale Dual Stage Axial Turbine (DSAT) and small scale Single Stage Radial Turbine (SSRT) was considered. From the application's view point, it is essential to design an appropriate turbine, from the mentioned categories, which is capable to work in an efficient way especially at the off design circumstances.

With the aim of decreasing losses of small scale axial turbine by using the multi-objective function, Bahr Ennil et al [12] uses and improved some loss correlations. They concluded that the Kacker & Okapuu loss model is able to predict effectively the closest losses to those from the CFD in the SSAT. Moreover, the authors concluded that the optimization technique can be employed to reduce total loss by enhancing the overall design for the all turbine. However, in the mentioned research, the axial turbine and also only single stage was the one of interest by the authors. Similar studies about various types of losses' models that associated with different types of turbines were comprised in the literature [13- 15].

Similarly, single stage axial turbine for ORC cycle was studied by Martins at al [16] in order to analysis and enhances its performance. The authors were able to propose a loss model for clarifying the flow losses and they concluded that the profile of convergent-divergent nozzle has a better performance especially at high working temperature of the evaporator.

Recently, the thermodynamic analysis for hybrid, gas, ORC and absorption refrigeration, cycles has been achieved by Mohammadi et al [17]. In their study different parameters such as pressure ratio, inlet fluid temperatures were investigated. The authors concluded that at the on design conditions, the studies system was able to form up to 30kW and around 8kW cooling power with about overall efficiency of about 67%. However, the authors mainly focused on the cycle analysis without any simulation to any of the system's components and also they did not considerate to the design of turbine.

Some studies tried to optimize the turbine performance by considering single or multi objective function optimization through both the stator and rotor for the two types of turbines [18-20]. Those studies have showed a valuable enhancement in the turbine efficiency by modifying the blade shapes and their numbers where the highest efficiency was achieved in [19]. With a 4.58 inches rotor diameter and 7 pressure ratio of radial gas turbine, the power output ranged from 50 to 100 hp was achieved in the study done by Jones [21]. Up to 88% and 86% total to total and total to static efficiencies respectively for the studied radial turbine were achieved.

The exergy and energy analyses for combined cycles under the off design conditions was accomplished by Chen et al [22]. The authors found that the off design conditions give more accurate

results in terms of the investigated cycle performance. However, in their study neither the turbine design nor the any CFD simulation was considered.

An intensive parametric study to the three types of micro turbine, single stage axial, radial inflow and radial outflow turbines, for ORC cycle and Brayton cycle applications has recently been established by Al Jubori et al and Daabo et al respectively [23- 25]. The authors studied different parameters for both the turbine and cycle with the sake of improving the cycle performance by escalating the turbine efficiency. In their study different working fluids were also examined for the ORC cycle.

The performance of radial turbine working on two different working fluids, R245fa and R1233zd, for truck application was experimentally investigated by Guillaume et al [26]. In their study the authors evaluated the ORC turbine performance in terms of the reduction in the mass of working fluid with respect to pressure ratio, produced power from turbine and the net output power from the cycle.

In this work, an integrated methodology is established. It chains mean line design and 3D CFD simulation of efficient Small Scale Turbines SST. Furthermore, it compares two types of SST in, Dual Stage Axial Turbine DSAT and Single Stage Radial Turbine SSRT in order to figure out the performance of each style using various boundary conditions. By the end of this study the most suitable type, for the solar Brayton cycle application, of the three investigated configurations, in both the on and the off-designs conditions, can be known. To determine the preliminary dimensions and performance of each type the mean line proposal design for each turbine's type was established using the Engineering Equation Solver (EES) code [27]. After, the mean line has been integrated with ANSYS CFX [28] in order to comprehend the 3D turbines and assess the performance of each one. As a result, the values of their efficiencies were built depending on the thermodynamic operating conditions and then directed to the cycle in order to pick up their influence on the overall cycle thermal efficiency. All in all, this study pursues to identify a suitable turbine to come across all the operating conditions of the cycle and identify the effect of each; the turbine and the compressor on the cycle performance. Furthermore, a brief studying on some types of losses such as the trailing edge and the tip clearance as well as evaluating the overall losses in terms of the loss coefficient have also been covered in the present study.

2- Brayton Cycle

One of the main advantages of conventional thermal Brayton cycle is using the compressed air as a working fluid so it is accounted as a clean cycle and does not affect the environment. However, the compressed air needs to be at high level of temperature in order to achieve the potential energy which is required to raise the fluid enthalpy. This heat off course can be applied through the combustion chamber which uses different types of fuel and as a result, this cycle in its current characteristic, does not considered as complete environmentally friendly cycle.

As shown in figure 1, the proposal reheated solar thermal Brayton cycle contains: a compressor to raise the pressure of the working fluid; a thermal receiver for heating the compressed air (instead of combustion chamber); a turbine to transfer the air potential energy to mechanical energy; and final component is recuperator which is a heat exchanger to take advantage from the exhaust energy, if not, it would be lost to the environment. In figure (1A) the T-s (temperature-entropy) diagram is demonstrated [29].

The main function of the recuperator is to preheat the incoming air which is normally cold before pass into the heat source. The power required by the compressor can be calculated using the following equation [30]:

$$W_C = \frac{Cp\, T_1(R_C{}^{\gamma} - 1)}{\eta_C} \quad (1)$$

Where Cp is the air specific heat constant at constant pressure, T1 is the air temperature at the compressor inlet, $R_C = P_2 / P_1$ is the compressor pressure ratio, γ is the specific heat ratio and η_C is the compressor efficiency.

The specific heat, working fluid per unit mass, supplied from the thermal solar receiver is:

$$Q_{Net} = Cp(T_4 - T_3) \quad (2)$$

The working fluid going away from solar receiver would have the required potential energy from both; the compressor and the thermal receiver will passes through the turbine in order to generate power output which is given by:

$$W_T = Cp\, \eta_T T_4 \left(1 - R_T{}^{-K}\right) \quad (3)$$

Where η_T, is the turbine efficiency, T_4 is the air temperature left the turbine, $R_T = P_4 / P_5$ is the pressure ratio in the turbine and K is γ-1/γ.

Supposing that the coefficient of pressure loss is X, and then equation 3 will be written as:

$$W_T = Cp\, \eta_T T_4 (1 - (XR_c) - K) \quad (4)$$

When the working fluid leaves the turbine to the atmosphere, it will move across the recuperator. The heat gained (Q_G) by incoming compressed air and the heat rejected (Q_R) through the leaving air is given by the next two equations respectively:

$$Q_G = \dot{m}(h_2 - h_3) \quad (5)$$

$$Q_{cRej} = \dot{m}(h_5 - h_2) \quad (6)$$

The effectiveness, ε, can be defined as following:

$$\varepsilon = \frac{h_3 - h_2}{h - h_2} \quad (7)$$

The net, useful, power output that can be gained from the preheated Brayton cycle can be determined by using the next formula:

$$W_{net} = W_T - W_C \quad (8)$$

The above equation can be reformulated to become:

$$W_{net} = Cp\left[\eta_T T_4 (1 - (XR_c) - K) - \frac{T_1(R_C K - 1)}{\eta_C}\right] \quad (9)$$

The efficiency of the thermal Brayton cycle (η_{th}) is:

$$\eta_{th} = \frac{W_{net}}{Q_{Net}} \quad (10)$$

Equation 10 can also be written in terms of pressure ratio, turbine efficiency, compressor efficiency, recuperator effectiveness and temperatures to be as following [30]:

$$\eta_{th} = \frac{\eta_t T_4\left(1-(XR_{c)}{}^{-K}\right) - T_1\left(\frac{R_c^{K-1}}{\eta_c}\right)}{T_4\left(1-\varepsilon\left\{1-\eta_t\left(1-(XR_{c)}{}^{-K}\right)\right\}\right) - T_1(1-\varepsilon)\left(1+\left(\frac{R_c^{K-1}}{\eta_c}\right)\right)} \quad (11)$$

As it is shown in the above equations as well as figure 1, the cycle components; each component of these elements needs to be sensibly designed so that the overall cycle efficiency increases. In this research only the choice of the best design parameters of the turbine, which leads to higher turbine isentropic efficiency and power output, will be discussed. This without doubt will improve the overall efficiency of the all system performance.

3- Axial and Radial Turbines

There are many factors need to be carefully studied when one wants to determine whether the axial or the radial turbine is the one of interest in a specific application. Possibly the manufacturing constraints, the cost production, the suitability to the specific application and the mechanical integrity, are among the main factors which determine which type will be more suitable. The following table, Table 1, gives the most important and brief differences between the axial and radial turbines [31-37].

Table1. Main features of SST.

Efficiency	The peak efficiency levels for the two stages are nearly identical, capability of the work done per stage.	For low mass flowrate, its efficiency is higher than the axial flow turbine. The two stage types offer similar efficiency possibility.
Power output	Greater flow capacity per unit frontal area of the axial-flow stage. However, the work done is lower than the radial flow turbine.	Is able to extract higher output power as a result of the high length and curvature of the rotor blades. This contributes in having greater pressure ratio, 4 per stage, with lesser flow rate values
Manufacturing	It can reach a higher level of efficiency but higher the blade profile precision level will be then required.	Attractive for small units such as turbochargers and micro-turbines. It is very compact.
Design	The rotor tip diameter is the factor used in defining the axial-flow stage's frontal area.	The nozzle outer diameter is the parameter used for determining the radial-inflow stage.
Analysis	The aerofoil analysis, which two dimensional analysis, is the one followed during the analysis.	The one-dimensional or preliminary design method is the most effective approach in analysing its performance.

Operational life	Higher operational life compared to the radial flow turbine.	Higher operational life as a result of being lesser mechanical and thermal stress because the fluid hits the rotating shaft perpendicularly.
Commercial availability	Both; the multi stage and the single stage are commercially available	Single stage applications are more common than the multi stage.
Cost	The single stage has lower cost, lower design complexity and ease of maintenance.	The one-dimensional or preliminary design method is the most effective approach in analysing its performance.
mechanical integrity	Greater flow capacity per unit frontal area of the axial-flow stage.	Fewer blades per blade row, which can offer a major cost advantage, in particular in the smaller sized units.
Off design conditions	At low blade rotational speed the SSAT has the ability to behave better than the SSRT at the off design conditions.	The optimum achieved efficiency for the SSRT corresponds to a higher rotational speed than that for the axial one.

4- Governing Equations

4.1 Mean line Design of the Axial Turbine

The first and the essential step in the turbines' design procedure is the mean line, the one dimensional analyses. So, the three dimensionless factors (flow coefficient, loading coefficient and degree of reaction) are essential to be selected and in this manner the preliminary velocity and triangles efficiency will be determined. Figure (2) shows the velocity triangles in both the axial and the radial turbines. The working fluid, compressed air, comes in the nozzle with an absolute velocity (C_1) and a flow angle (α_1) and then departs it at absolute velocity and flow angle (C_2) and (α_2). The other remaining sides and angles represent are the inlet and outlet relative velocities and angles (w_2, w_3, β_2 and β_3 respectively). Some of the most relating correlations and equations which have been used in the axial turbine design are arranged below [31-41]:

The loading coefficient Ψ and flow coefficient $\emptyset$ can be determined by equations 12& 13 respectively.

$$\Psi = \frac{C_{\theta 2}}{U_2} \tag{12}$$

$$\emptyset = \frac{C_{m3}}{U_2} \tag{13}$$

The inlet, outlet blade angles and flow angles can then be obtained using equations 14 and 15 respectively.

$$\left.\begin{aligned}\tan\beta_2 &= \frac{(\Psi - 2R_n)}{2\phi}\\ \tan\beta_3 &= \frac{-(\Psi + 2R_n)}{2\phi}\end{aligned}\right\} \quad (14)$$

$$\left.\begin{aligned}tan\,\alpha_3 &= \frac{-(\Psi/2-(1-R_n))}{\phi}\\ tan\,\alpha_2 &= \frac{(\Psi/2+(1-R_n))}{\phi}\end{aligned}\right\} \quad (15)$$

The nozzle loss coefficient (ζ^*) and the manufacture losses such as the tip clearance ε one can be defined in equations 16 to 18. Where ε_x and ε_r represented the axial and radial clearances respectively, ζ_1 are nozzle loss coefficient value.

$$\zeta^* = 0.04 + 0.06\left(\frac{\varepsilon}{100}\right)^2 \quad (16)$$

$$\varepsilon = \varepsilon_x + \varepsilon_r \quad (17)$$

$$1 + \zeta_1 = (1 + \zeta^*)\left(0.996 + 0.021\frac{B}{H}\right) \quad (18)$$

Similarly, the associated loss coefficient in the rotor part of the turbine $\zeta_2$is sorted in equations 19.

$$1 + \zeta_2 = (1 + \zeta^*)\left(0.975 + 0.075\frac{B}{H}\right) \quad (19)$$

The losses in pressure can be evaluated using the correlations of pressure coefficients for each the stator and the rotor are shown in equations 20& 21:

$$Y_N = \frac{(P_{01}-P_{02})}{(P_{02}-P_2)} \quad (20)$$

$$Y_R = \frac{(P_{03\,rel} - P_{04\,rel})}{(P_{01\,rel} - P_4)} \quad (21)$$

After calculating all the associated losses in the both parts of the axial turbine, the total to total, in case of more than one stage, can be calculated as in equations 22 and total to static, in case of single stage turbine, can be determined using equation 23.

$$\eta_{tt} = \frac{1}{1 + \left[\zeta_R\, w_3^2/2 + \left(\zeta_S C_2^2/2\right)\right]/\Delta W} \quad (22)$$

$$\eta_{ts} = \frac{1}{1 + \left[\zeta_R\, w_3^2/2 + \left(\zeta_S C_2^2/2\right)\left(\frac{T_3}{T_2}\right) + C_3^2/2\right]/\Delta W} \quad (23)$$

The blade number and height are Z and H respectively can be specified using the next two formulas:

$$Z = \left(\frac{\pi}{30}\right)(110 - \alpha_1)\tan\alpha_1 \quad (24)$$

$$H = r_t - r_h \quad (25)$$

Where r_t and r_h represented the tip and the hub radius values of blades.

4.2 Mean line Design of the Radial Turbine

Using the same approach of that mentioned in the axial turbine, the loading coefficient and the flow coefficient of the radial turbine should be firstly determined as a starting point in the design procedure, as showing in equations 26 and 27 respectively[28-38]:

$$\Psi = \frac{\Delta h_{actual}}{{U_4}^2} \quad (26)$$

$$\emptyset = \frac{C_{m5}}{U_4} \quad (27)$$

The tip diameter and the rotor vanes number can be calculated using equations 28 and 29 respectively

$$r_{5_t} = \sqrt{\frac{A_5}{\pi} + r_{5hub}^2} \quad (28)$$

$$Z_{rotor} = \frac{\pi}{30}\,(110 - \alpha_2)\tan(\alpha_2) \quad (29)$$

The enthalpy drop because of the tip clearance is consisting of the axial clearance and radial clearance. The value of this drop can be determined by using the next correlation:

$$\Delta h_{tip,clearnace} = \frac{U_3^4\, Z_{rotor}}{8\pi}\left(0.4\,\varepsilon_x C_x + 0.75\,\varepsilon_r\, C_r - 0.3\sqrt{\varepsilon_x \varepsilon_r C_x C_r}\right) \quad (30)$$

The two values of clearance can be calculated after calculating the axial and radial values of the absolute velocity, as shown in the next two equations:

$$C_x = \frac{1 - \left(\frac{r_{5tip}}{r_4}\right)}{C_{m4}\, b_4} \quad (31)$$

$$C_r = \left(\frac{r_{5tip}}{r_4}\right)\frac{l_{rotorx} - b_4}{C_{m5}\, r_5 b_5} \quad (32)$$

Where the rotor length can be determined using the formula shown in equation 33

$$l_{rotorx} = 1.5\left(r_{5tip} - r_{5hub}\right) \quad (33)$$

So, using the following correlation, the two values of clearance can be computed:

$$\varepsilon_x = \varepsilon_r = 0.04\left(r_{5tip} - r_{5hub}\right) \quad (34)$$

The secondary losses are estimated by using the next equation:

$$\Delta h_{secondary} = \frac{C_4^2 \, d_4}{Z_{rotor} \, r_C} \tag{35}$$

The loss value associated with the exit kinetic can be assessed using the following equation,

$$\Delta h_{exit} = 0.5 C_5^2 \tag{36}$$

Regarding the loss from the nozzle, this loss can be determined after tracking down the moody chart and find out the value of friction factor$f$, the differences in the enthalpy due to the friction effect.

$$f = 8\left[\left(\frac{8}{Re}\right)^{12} + \left(\left[2.475 \ln\left(\frac{1}{\left(\frac{7}{Re}\right)^{0.9} + 0.27PR}\right)\right]^{16} + \left[\frac{37530}{Re}\right]^{16}\right)^{-1.5}\right]^{\frac{1}{12}} \tag{37}$$

$$\Delta h_{friction,nozzle} = 4 f_{nozzle} \bar{C}^2 \, \frac{l_{hyd,nozzle}}{d_{hyd,nozzle}} \tag{38}$$

The losses which are accompanying to the volute geometry can be valued using the following correlation:

$$\Delta h_{loss,volute} = \frac{r_{volut} \, C_2^2}{2} \tag{39}$$

After finding all of the earlier mentioned losses, the total enthalpy losses will be determined by via equation 40.

$$\Delta h_{loss,total} = \Delta h_{loss,volute} + \Delta h_{friction,nozzle} + \Delta h_{tip,clearance}$$
$$+\Delta h_{secondary} + \Delta h_{frictio} + \Delta h_{exit} \tag{40}$$

Finally, the total to total efficiency will be calculated as shown in equation 41.

$$\left(\eta_{turbine,stage,ts}\right)_{new} = \frac{\Delta h_{actual}}{\Delta h_{actual} + \Delta h_{loss,total}} \tag{41}$$

The mentioned correlations and equations are the most famous ones which can be used in order to design and estimate the overall turbine efficiency. The flow chart of preliminary design is presented in figure 3. The boundary conditions BCs and the dimensions of each turbine's geometry are organized in table 2 and table 3 respectively. Moreover, the full details of the blade angles and dimensions are explained in figure 4.

5- Numerical Analysis

5.1Blade Generation

Once the mean line design has been performed, the next step was to build the geometry of each blade. That can be achieved by employing the three dimensional blade generations, Blade-Gen, in ANSYS Workbench. This feature was used to visualize blade of both the stator and rotor for the SSAT, DSAT and SSRT in two as well as three dimensions as shown in figures 5A, B and C respectively and to construct the complete stage geometry of each turbine's configuration. The fluid domain at the inlet and exit of each; the stator and the rotor and also the fluid passage both the stator and the rotor for each stage and turbine should be specified and applied in this step specifically. The solution quality, the accuracy and the computational costs, is influenced significantly by the domain discretization.

5.2 Mesh Generation

Once the overall geometry and mean line results being satisfied, the geometry of each blade transfers to what is called CFX Turbo-Grid feature in the ANSYS Workbench. The main function for the Turbo-Grid is to divide both the blade geometry and the fluid domain which was initiated in the Blade-Gen in to the required number of elements. Figures 6A, B and C show the 3 dimensional meshes for the used blade to blade passage for each; the SSAT, DSAT and SSRT respectively.
It is worth to mention that the grid size was varying depending on the zone of the blade, for example the grid size was refined in the areas near the surfaces of blades and the walls in order to keep up an acceptable compromise between computational costs and solution accuracy. In order to make sure that the satisfied element size has been chosen, the grid sensitivity investigation with respect to turbine efficiency was established as shown in figure 7.

5.3 Numerical Solution

It is well known that choosing the correct model for solving the required equations is one of the crucial tasks which need to be carefully considered. A wall treatment was automatically applied during the simulation in order to take in consideration the effects of all the walls. The main function of this wall treatment is to ensure smooth shift between low-Reynolds number and wall functions formulation through computational grids without any deficiency in accuracy [42]. In order to examine the distance between the first node and the wall, a dimensionless distance from the wall called y^+ is initiated. This method enables users from correctly specifying the near wall spacing according to the required value of y^+ for example near the passage or hub/ shroud tip. It can be defined as shown in equation 42:

$$\Delta y^+ = \frac{\Delta y \, Re_L}{\left[8.944 \, L \, (Re_x)^{1/14}\right]} \tag{42}$$

Where Δy^+ is the specified target y^+value, L is the blade chord, Δy is near wall spacing, Re_L and Re_{Lx} are Reynolds number values based chord length and the distance along the chord, computed from the leading edge, respectively.

Even though some models such as the Baseline BSL model has the ability to consider the advantages of other models in terms of the solution accuracy, it is still in fact unable to accurately predict the exact amount of separation especially for smooth surfaces. Moreover, the main problem with Wilcox model is its high sensitivity to the freestream conditions. By contrast the k-ω based on SST model is able to precisely predict the mention phenomena under pressure gradients.

For the current study and based on the turbulence model, the Shear Stress Transport (SST) k-ω model was employed to take into consideration the flow separation effect on the turbulent viscosity (eddy-viscosity).

The k-w based SST model is more accurate and reliable for a wide range of flows like airfoil, adverse pressure gradient and transonic shock waves. The k-ω transport equations are:

$$\frac{\partial}{\partial t}(\rho k) + \frac{\partial}{\partial x_i}(\rho k u_i) = \frac{\partial}{\partial x_j}\left(\Gamma_k \frac{\partial k}{\partial x_j}\right) + G_k - Y_k + S_K \quad (43)$$

$$\frac{\partial}{\partial t}(\rho \omega) + \frac{\partial}{\partial x_i}(\rho \omega u_i) = \frac{\partial}{\partial x_j}\left(\Gamma_k \frac{\partial \omega}{\partial x_j}\right) + G_\omega - Y_\omega + S_\omega \quad (44)$$

Where G_k , Y_k and S_k are the generation of turbulent kinetic energy, the fluctuating dilation and the source term of the k-w turbulence model. Similarly G_w, Y_w and S_w represent the dissipation rate of turbulent kinetic energy, the fluctuating dilation in compressible turbulence and are the source term of the k-w turbulence model.

5.4 CFD Simulation

By choosing the correct element type, element size and the solver, the model becomes ready to be simulated by using the 3D turbulent viscous flow in ANSYS-CFX solver. The used setting and the assumptions are suggested by [43] and they are as follows:

1- In the ANSYS-CFX solver each; the machine type (whether it is axial or radial), the rotation axis and the analysis type (whether it is steady state or transient) was selected from the basic settings [28].
2- The component (whether it is stator or rotor) definition is the next step where the passages alignment, the flow direction, wall configuration (whether there is a tip clearance at the shroud and the hub or not) and the rotor rotational speed were arranged.
3- Next, the fluid viscosity, phase and compressibility were put to rights. Furthermore, the compressed air as an ideal gas and the first order upwind advection scheme was chosen for the topology as it is numerically stable [28].
4- The Generalized Grid Interface GGI feature of CFX was selected to connect the components of the stage (stator and rotor in SSAT and SSRT) or even stages together (as in the case of DSAT) to make it ready for the shear stress turbulence model and with Navier-Stokes equations [28].
5- In order to enhance simulation accuracy, the mean value of y^+ was kept back at around unity as recommended in the CFX-Solver theory guide [28].
6- In the physics definition scheme, air as ideal gas for the working fluid type was selected and the chosen inlet and outlet boundary conditions are: the total pressure, the total temperature and the flow direction as inlet conditions. By contrast, the static pressure was selected to characterize the outflow [28].
The procedure for the CFD simulation steps is shown as block diagram in figure 8.

The convergence standards for the residuals of the velocity, the continuity and the energy equations were set to the order of 10^{-5}, 10^{-5} and10^{-6} respectively and once the solutions were met with the convergence criteria, the results became ready to be analysed.
The best distributions of the velocity through all the stage for the each of the three configurations, SSSSAT, DSSSAT and SSSSRT, is achieved and presented in figures 9 A, B and C correspondingly. In the same way the pressure distribution, Blade-to-Blade view, along each complete stage of three earlier configurations of the studied turbines have shown in figures 10 A, B and C respectively.
Moreover, the load distributions on each the Pressure Side (PS) and the Suction Side (SS) through the all stage of the non-dimensional meridional coordinate at the studied pressure ratios (2, 3 and 4) for

the SSAT, DSAT and SSRT respectively are also presented figures 11 A, B and C. In these figures the differences between the pressure of the SS and PS is in fact represents the amount of load occurs on blades which has been increased with increasing the pressure ratio. Also, it is clear that the behaviour is dissimilar between the three investigated of turbine configurations. Moreover, it can be seen that the differences between SS and PS is varying through the stage and at each specific turbine's configuration. For example, the heaviest load, the highest difference, was noticed to be at the shroud region for the axial turbine; however, the opposite is the case in the hub area. The temperature spreading, Blade-to-Blade views, along each complete stage of three previous configurations of the considered turbines have shown in figures 12 A, B and C in that order.

6- Validation of the current study

Even though the Computational Fluid Dynamics CFD is considered as a one of the most reliable methods which cover the analysis for different fields, it is still a general simulation tool which needs to be validated experimentally. Hence, the results obtained from the current study by using these tools are not reliable unless they are compared an experimental work either for the same model or with the experimental models of some other researchers. So, in order to justify the current results and because the experimental work of the current research has not been completed yet, the authors have successfully modelled the complete design for two different experimental studies from literature [44 & 45]. Among the many experimental studies found in literature [44-51], only two studies have been chosen to get on to the validation of the present study. The two mentioned studies were specifically chosen as a result of having a relatively sufficient data in order to make the mission of designing and modelling their prototype is reachable. Here, it is worth to mention that the experimental study which has been found in reference [44], which has been established in the lab using small scale axial turbine, was modelled and analysed using the a full three dimensions analysis. Furthermore, the second validation, with reference [45], the full three dimensions analysis was established as most of the required data were on paper of that study. Figures 13 A displayed the results of the comparison between the current three dimensions CFD model and the experimental work done using the lab found in [44]. By contrast, the results of the three dimensions analysis were figured out in figure 14 B. All in all, the validation results showed an excellent agreement has been achieved between the current work and the two chosen ones especially with the model of [44] with no more 16.5 % and less than 10 % deviation values for the second model. At this point it is worth to mention that the uncertainty in the results belongs to some errors such as the blade's surface roughness, state flow condition, which is not purely steady in reality, and some unconsidered losses, by the CFD model, like the mechanical losses.

7- Results and Discussions

This section will figure out and analyse the results of the 3D turbulent viscous flow model for the three configurations of the SST by using ANSYS-CFX solver. Consequently, the on design and the off design conditions for each of the three different patterns at different factors such as the rotational speed, inlet temperature and pressure ratio were investigated in order to figure out the performance of each turbine in terms of its efficiency and power output.

7.1 Boundary conditions

Assessing the power output, it has been seen that in general, this factor has shown a strong dependence on the value of the pressure ratio and that was for the studied inlet air temperatures of (400K to 600K). Moreover, this factor, the pressure ratio, has almost same influence on the two configurations of the studied SST. As for the rotor rotational speed, it can be noticed that the power

output of each turbine increased until a certain value of rotational speed, which seems to be the optimum value, and then begins to decline. Moreover, comparing to its lowest rotational speed, at 60,000 RPM, the power output developed to be about 130% of the power output at the optimum value of the rotor rotational speed. Furthermore, the value of optimum rotational speed varies depending on the turbine configuration and its supplied pressure ratio value.

For the sake of accuracy, the power out form has been divided by the mass flow rate of the working fluid, compressed air, for all the following results, as there was a slight difference in the mass flow rate value.

Figure 14 displays the consequence of the rotor rotational speed on the turbine power efficiency and output for the DSAT and SSRT at a temperature of 400K and a turbine pressure ratio ranged from 2 to 4. In comparison with SSRT it was noticed that the DSAT demonstrated higher efficiency for all the rotational speeds and at all the investigated inlet temperature values. This indicates its ability to work more effectively at the off-design conditions. The reason for that could relate to the peripheral speed which is high so, the turbine exit flow will be supersonic. The difference between the SSAT and DSAT became higher which might be because of the higher Mach numbers at the trailing edge part of the blade which leads to a fall in the efficiency at higher PR. In other words, the peripheral speed will be high and that means that the exit flow will experience supersonic which might not be the case for the DSRT. This can indicated the relation between the losses and both rotational speed and the pressure ratio as well.

As the rotational speed increased the difference between the two efficiency trend lines relatively decreased. That is because increasing the rotational speed of SSRT allows a reduction in both the secondary and leakage losses. The maximum efficiency for SSRT, at 70 KRPM, was approximately 81.5% at PR of 2. However, it can be also seen that the tipping point was at 100 KRPM and the maximum divergence from the optimum efficiency was recorded to be about 17 % for the SSRT with only about 3% for the DSAT.

Although the Small Scale Axial Turbines DSATs displayed higher efficiencies, its power output of experienced lower values compared to SSRT through all the rotational speeds, except 110 KRPM. The reason for that was the ability of radial turbine of extracting higher power at the same value of mass flowrate. The maximum variance in the power output between both turbines was noticed at minimum rotational speed of 60 KRPM was ranged from 60 KRPM to 90 KRPM for the three studied values of pressure ratio. Similarly, as the rotational speed increased the difference between the value of power output decreased, until they were closely matched at and after 107 KRPM. That was because of the sudden drop of the out power for SSRT. The peak power output, as a specific work, at a pressure ratio of 2 were around 49 J/s and 55 J/s at 90 KRPM and 75 KRPM for the SSDSAT and SSRT respectively. As for the PR of 3 and 4, the corresponding values of the specific work extracted from the three patterns were approximately 61 J/s and 66 J/s, 85 J/s and 100 J/s for the SSDSAT and SSRT respectively. This indicates the importance of pressure ratio in terms of the amount of obtained power for all the two turbines' pattern.

Similarly, figure 15 displays the effect of the rotor speed on the turbine efficiency and power output for the DSAT and SSRT at PR from 2 to 4 and compressed air inlet temperature of 500 K. In this figure, it can be noticed that in spite of the efficiency value the DSAT hit the top at rotational speed of 90, KRPM with about 84.5%. The performance of the SSRT on the other hand was not good in terms of the efficiency which was increased from about 67% to 81% during the investigated range of rotor rotational speed at PR of 2 while the its efficiency hit the tip at PR of 3 with around 84.5% as it was

working with the on-design conditions. Again the DSAT showed better behaviour during the off design conditions than the other investigated type of turbines. The other important outcome from this figure is that the advantage switched to the SSRT after the rotational speed of 95 KRPM because of the low values of both the secondary and leakage losses at higher rotational speed values.

As for the extracted power from the studies turbines, it can be seen that generally the power of the SSRT was the highest during all the investigated pressure ratio values. Specifically, at PR of 2 the power for DSRT and SSRT were approximately 57 J/s and 71 J/s. In the same way the trends of output power values for the two turbines' types were represented in the same figure to show around 13% and about 23% maximum differences during the off design operation. Having said that the maximum power output in terms of Enthalpy were about 76 J/s and 99 J/s at the same rotational speed of 90 KRPM, indicating that the two turbines were working at their nominal conditions. For PR of 4, the increment in the amount of power output at high rotational speed has shown higher differences between the one extracted from the SSRT compared to the DSAT. In terms of numbers, the maximum corresponding extracted specific work for each; the DSAT and SSRT were in the region of 81 J/s and 113 J/s respectively.

The outcome of changing the rotor rotational speed on the turbine power efficiency and output for the two features DSAT and SSRT at a temperature of 600K and a turbine inlet temperature ranged from 2 to 4 is figured out in figure 16. General speaking, at this specific level of fluid temperature it can be seen that the high level of efficiency was switched to the SSRT especially at the high rotor rotational speed with a certain fluctuation point, normally higher than 95 KRPM. Again this gives an indication on the relation between the losses and both pressure ratio and the rotational speed. As for the other turbine, the results showed that at 3 and 4 the radial demonstrated relatively higher efficiency especially between 70 KRPM and 90 KRPM.

During all the studied values of pressure ratio, a maximum of about 11 % differences between the highest and lowest values of turbine efficiency was put on show at a very low rotational speed of 60 KRPM. As the rotational speed increased the difference between the two efficiency trend lines diminished, until they were closely matched at around 105 KRPM. That was because increasing the rotational speed of SSRT allows a reduction in both the secondary and leakage losses. The efficiency pointed for DSAT at 90 KRPM was approximately 83.5%; this may be due to that this range of the rotational speed was with the limit of nominal conditions, whilst for SSRT the maximum was noticed at 70 KRPM with approximately 81% at PR of 2. However, it can be also seen that the tipping point was at 100 KRPM and the maximum divergence from the optimum efficiency was recorded to be about 11% for the SSRT compared to around 6% for the DSAT.

Even though the DSAT demonstrated higher efficiencies, the achieved power output had lower values compared to SSRT through all the rotational speeds especially at higher rotational speed, more than 95 KRPM. The reason for that was the ability of radial turbine of extracting higher power at the same value of mass flowrate in particular at high fluid temperature. As the rotational speed increased the difference between the value of power output increased. In terms of number, the extracted output power for the SSRT reached approximately 1.7X of that achieved by the DSAT. Furthermore, the ultimate power output values, as a specific work, at a pressure ratio of 2 were around 67 J/s and 85 J/s at 90 KRPM for the DSAT and SSRT respectively. As for the PR of 3 and 4, the corresponding values of the specific work extracted from the three patterns were approximately 91 J/s and 93 J/s, 128 J/s and 135 J/s for the DSAT and SSRT respectively. This indicates the importance of pressure ratio in terms of the amount of obtained power for all the two turbines' pattern.

7.2 Tip Clearance and Trailing Edge Losses

One of the main restrictions in the small scale turbines industry is the limitation of the manufacture concerns such as the tip leakage losses which is reflected directly to the amount of pressure losses and as a result on the their efficiencies. Losses in any real system are inevitable. One indicator of losses can be the property of entropy or the entropy generation which leads to decrease the overall system efficiency or performance, see for example the difference between the two flow behaviours in figure 17. In gas turbines losses are associated with either the turbine structure like the skin friction losses or the flow circumstances of the turbine working fluid like the endwall flows which is one of the forms of the secondary flows which are the main sources of recirculating flow and generating what is known as passage vortex. Like this flow behaviour occurs mainly in the radial flow turbines as a result of their blades' complexity compared to the axial flow turbines. To tackle this problem, both; the blade geometry and the rotor rotational speed need to be carefully studied.

Before starting the effect of some parameters on the dual stage turbine, figure 18 gives an indicator about the ratio of power output at each stage of the DSAT at different rotational speed values. The amount of power extracted from the second stage was higher because of the higher pressure ratio in this stage. The effect of each the stator trailing edge and the rotor shroud tip clearance on the amount of losses are established in the section to see their effect on both the efficiency of the power output of the dual stage axial turbine where this effect has higher influence because of the connection between the two stages. It is worth to mention that this analysis has been done at only one boundary condition i.e. the nominal design condition for the sake of abbreviation. In figure 19; both the efficiency and the power output of each stage alone was higher with low tip clearance and lower values of stator trailing edge, having said that, the dual stage configuration showed higher influence to the stators' trailing edge values than those of the rotors' tip clearance. The reason for that is the importance of matching the stator trailing edge of the first stage with the rotor leading edge of the second stage which otherwise motivates other types of losses such as the secondary losses which arise during the flow turning inside the passage. The other outcome from this investigation is that while the efficiency of each stage separately was relatively higher influenced than the dual stage. On the other hand, as there is only single stage radial turbine analysed in this study, the rotor's tip clearance was by far the most influence parameter on the performance of the SSRT.

In terms of number, it can be seen that while the maximum difference in the efficiency values in each stage separately was around 1.5 % when tip clearance increased from 0.3 to 0.4 mm, while this difference reached less than 1% in the dual stage. Similarly the efficiency of each stage separately was around 1.3 % when trailing edge thickness became 0.5 mm while this factor did make larger effect in the dual stage efficiency when the relevant difference in the efficiency was about 2.2 %. This however, indicates the important of matching the trailing edge of the first stage rotor, which was fixed at 0.3 mm during this study, with the leading edge values of the second stage stator. The relevant figures of the power output of each stage separately as well as the dual stage have been attached near the figures of the efficiency. Similarly, the maximum sacrifice in the efficiency value in the SSRT was less than 0.2 % by increasing the stator trailing edge but this value became around 1.5 % with increasing the rotor tip clearance. The power output showed almost similar influence to each; the trailing edge and tip clearance with about 275 and 199 W lower when they increased to 0.5 mm each.

7.3 Loss Coefficient

Finally the overall losses coefficients of each of the three configurations at different boundary conditions have been briefly discussed in this section. Many studies have been published on the both the characterizations and the methods of calculation for different types through various correlations as

previously shown in section 3. In turbines, losses can be divided to those which takes place in the stator and those happens in the rotor part, more details can be found in [12, 52-55]. In the current study the loss coefficients in terms of pressure losses, as one significant indicator of losses, for each of three configurations and at different working circumstances will be evaluated and discussed next. Using the equations mentioned in section 3, the pressure loss coefficients have been used to predict the losses in the total pressure for both the stator and rotor of each of the three investigated turbine features for the numerous examined boundary conditions is presented in figures 20 A-C.

The overall indications of these figures showed that by increasing each the fluid inlet pressure temperature, the value of pressure coefficient increase. Moreover, these values experienced their lowest magnitudes at certain rotor rotational speed.

8- Brayton Cycle Results

After this long study the main outcomes from such as the turbine efficiency and the studied boundary conditions have been used as input parameters with the aim of predicting the Brayton cycle efficiency as offered in figures 21 A-C. The performances of some other cycle components for instance the compressor efficiency and the thermal receiver have also figured out.

It is clear from figure 21 that the maximum turbine efficiency the highest cycle efficiency is achieved. However, to have a relative At this point it is worth emphasising the importance of having relatively long-standing turbine efficiency, working at its designed is not applicable in reality. So, the other important factor is to investigate the off-design conditions at different boundary conditions and cycle components' efficiencies which have direct effect on the overall cycle efficiency. It is well known that the higher temperature at specific value of pressure ratio values the better overall efficiency of the cycle can be achieved. For the sake of accuracy, the effect of compressor efficiency on the overall cycle efficiency has been highlighted in this section. From the cycle analysis, it was found that at compressor efficiency of 95%, the cycle efficiency can be increased by about 4.5 % and 9.5 % by enhancing the efficiencies of the turbine from 80% to 90% when the fluid inlet temperature are 500 K and 600 K respectively. Of course these values can be changed based on the cycle boundary conditions such as the pressure ratio and the inlet temperature of the compresses air increased. On the other hand, the performance of the cycle can deteriorated up to around 7.5% if the compressor efficiency decreased from 95% to 85%.

9- Conclusion

In this paper, the performance of small scale turbines with two different patterns named as DSAT and SSRT working on compressed air as a working fluid have been considered and analysed at different boundary conditions with the aim of picking out the most appropriate turbine for the current application, small scale solar powered Brayton cycle. Their performance at both the on and the off design conditions were also examined. The results of the current work are confirmed using the results from the experimental work which has been established in the lab as well as other experimental work found in literature. From this extensive study some essential spots can be briefly offered below:

1- The dual stage axial turbine has the ability to behave better than the other two turbines at the off design conditions and this can achieve a relatively stable efficiency for the cycle. Having said that, the extracted output power was not sufficient when it is compared to the radial turbine.

2- The single stage radial turbine is superior when the main concern is to provide more output power compared to the other turbine at almost all the studied inlet temperature pressure ratio.

The output power reaches up to 1.7X of that extracted from the dual stage axial turbine especially at high pressure ratio.

3- The radial turbine is much affected by the tip clearance rather than trailing edge thickness. The tip clearance and trailing edge losses together contributed up to around 4 % and the latter can be reduced in the dual stage by carefully matching the rotor trailing edge of the first stage and the stator leading edge of the second stage.

4- The loss analysis showed that increasing each the fluid temperature and pressure ratio contribute in increasing the rotor total loss coefficients. Moreover, the SSAT showed the highest values for the mentioned coefficients and the SSRT experienced the lowest at certain rotational speed values.

5- At 95% compressor efficiency, the maximum improvement in the cycle thermal efficiency ranges from about 5% to 10%, depending on other boundary conditions, can be achieved if the turbine efficiency increased from 80% to 90% at fixed other boundary conditions. By contrast, a variation in the cycle efficiency reached up to 7.5% was noticed by changing the compressor efficiency between 95% and 85%.

After this study it is clear that the competition now is between the SSDSAT and the SSRT which could open the door for adding new configuration of turbine i.e. the Small Scale Dual Stage Radial Turbine SSDSRT which might be the topic of the future studies.

NOMECLATURE

Symbols

A	Area	**α**	Absolute flow angle (deg.)
b	Blade width (m)	**β**	Relative flow angle (deg.)
B	Axial chord (mm)	**θ**	Tangential/circumferential direction
c	Absolute velocity (m/sec)	**ε**	Clearance (m)
d	Diameter (m)	**η**	Efficiency (%)
f	Friction factor	**γ**	Specific heat ratio
h	Enthalpy (J/kg)	**υ**	Velocity ratio (-)
H	Blade height (mm)	**ρ**	Density (kg/m^3)
i	Incident angle (deg.)	**φ**	Flow coefficient (-)
k	Loss coefficient (-),	**ψ**	Loading coefficient (-)
K	γ-1/γ		
l	Length (m)	**ω**	Acentric factor (-)
m	Mass flow rate (kg/sec), Meridional	**ζ**	Losses (-)
p	Pressure (Pa)	**ζ^***	Nominal loss factor
PR	Pressure ratio	**Subscripts**	
r	Radius (m)	**1-6**	Station
r_C	Mean radius of curvature	**c**	Compressor
R_c	Compressor pressure ratio	**G**	Gained
		h	Hub
Re	Reynolds No. (-)	**hyd**	Hydraulic
R_n	Degree of Reaction	**m**	Meridional direction
s	Entropy (J/kg.K)	**r**	Radial, Rotor,
SC	Swirl coefficient (-)	**Rej**	Rejected
T	Temperature (K)	**rel**	relative
U	Rotor blade velocity (m/s)	**s**	Isentropic, Stator
w	Relative velocity (m/sec)	**t**	Total, Stagnation, Turbine, tip
W	Power (W)	**th**	Thermal
x	Pressure loss coefficient	**ts**	Total to static
Z	Blade number in radial turbine	**x**	Axial component

Acronyms

BCs	Boundary Conditions	**DSAT**	Dual Stage Axial Turbine
SST	Shear Stress Transport	**SSDSAT**	Small Scale Dual Stage Axial Turbine
CFD	Computational Fluid Dynamics	**SSRT**	Single Stage Radial Turbine
PD	Preliminary Design	**SST**	Small Scale Turbines,

RMS	Root Mean Square	**SSAT**	Single Stage Axial Turbine

ACKNOWLEDGMENT

The author would like to thank the Higher Committee of Developing Education in Iraq HCED for funding this project.

References

[1] Makower, Joel, Ron Pernick, and Clint Wilder. Clean energy trends 2006. Clean Edge, 2005.
[2] J. Perkowski, "China Leads the World in Renewable Energy Investment," Forbes, July, vol. 27, 2012.
[3] Bhaskar Roy and A M Pradeep. "Turbomachinery Aerodynamics", Department of aerospace engineering. IIT, Bombay. Online series of videos.
[4] Pei, Gang, et al. "Construction and dynamic test of a small-scale organic rankine cycle." Energy 36.5 (2011): 3215-3223.
[5] Le Roux, Willem Gabriel, Tunde Bello-Ochende and Josua P. Meyer. "Operating conditions of an open and direct solar thermal Brayton cycle with optimised cavity receiver and recuperator" Energy 36.10 (2011): 6027-6036.
[6] Le Roux, Willem Gabriel, Tunde Bello-Ochende and Josua P. Meyer. "Optimum performance of the small-scale open and direct solar thermal Brayton cycle at various environmental conditions and constraints" Energy46.1 (2012): 42-50.
[7] Daabo, Ahmed M., Saad Mahmoud, and Raya K. Al-Dadah. "The optical efficiency of three different geometries of a small scale cavity receiver for concentrated solar applications." Applied Energy 179 (2016): 1081-1096.
[8] Daabo, Ahmed, Saad Mahmoud, and AL-Dadah Raya. "Effect of open cavity configuration on solar receiver thermal performance." Extended Abstracts. 2016.
[9] Daabo, Ahmed M., Saad Mahmoud, and Raya K. Al-Dadah. "The effect of receiver geometry on the optical performance of a small-scale solar cavity receiver for parabolic dish applications." Energy 114 (2016): 513-525.
[10] Al-attab, K. A., and Z. A. Zainal. "Performance of a biomass fuelled two-stage micro gas turbine (MGT) system with hot air production heat recovery unit". Applied Thermal Engineering 70.1 (2014): 61-70.
[11] Kiaee, Mehrdad, A. M. Tousi, and M. Toudefallah. "Performance adaptation of a 100 kW microturbine". Applied Thermal Engineering 87 (2015): 234-250.
[12] Ennil, Ali Bahr, et al. "Minimization of loss in small scale axial air turbine using CFD modeling and evolutionary algorithm optimization." Applied Thermal Engineering 102 (2016): 841-848.
[13] J. Kammeyer, C. Natkaniec, J. R. Seume, "Influence of tip-gap losses on the stage efficiency of downsizing turbocharger turbines". Leibniz Universitaet Hannover, Institute of Turbomachinery and Fluid Dynamics, Germany. 10.1243/17547164C0012010023.
[14] Mohammed Alexin Putra and Franz Joos. " Investigation of secondary flow behaviour in a radial turbine nozzle". Helmut-Schmidt-University, University of the Armed Forces Hamburg, Germany. Journal of Turbomachinery. November, (2013), Vol. 135 / 061003-1.
[15] Klonowicz, Piotr, et al. "Significance of loss correlations in performance prediction of small scale, highly loaded turbine stages working in Organic Rankine Cycles." Energy 72 (2014): 322-330.
[16] Martins, Guilherme Leibsohn, Sergio Leal Braga, and Sandro Barros Ferreira. "Design optimization of partial admission axial turbine for ORC service." Applied Thermal Engineering 96 (2016): 18-25.
[17] Mohammadi, Amin, et al. "Thermodynamic analysis of a combined gas turbine, ORC cycle and absorption refrigeration for a CCHP system." Applied Thermal Engineering 111 (2017): 397-406.
[18] Yahya, S. M. Turbines compressors and fans. Tata McGraw-Hill Education, 2010.

[19] Daabo, Ahmed M., et al. "Development of three-dimensional optimization of a small-scale radial turbine for solar powered Brayton cycle application." Applied Thermal Engineering 111 (2017): 718-733.
[20] Al Jubori, Ayad, et al. "Three dimensional optimization of small-scale axial turbine for low temperature heat source driven organic Rankine cycle." Energy Conversion and Management (2016).
[21] Jones, Anthony C. "Design and test of a small, high pressure ratio radial turbine." ASME 1994 International Gas Turbine and Aeroengine Congress and Exposition. American Society of Mechanical Engineers, 1994.
[22] Chen, Qiang, et al. "The exergy and energy level analysis of a combined cooling, heating and power system driven by a small scale gas turbine at off design condition." Applied Thermal Engineering 66.1 (2014): 590-602.
[23] Al Jubori, Ayad, et al. "Development of micro-scale axial and radial turbines for low-temperature heat source driven organic Rankine cycle." Energy Conversion and Management 130 (2016): 141-155.
[24] Al Jubori, Ayad M., et al. "Modelling and parametric analysis of small-scale axial and radial-outflow turbines for Organic Rankine Cycle applications." Applied Energy 190 (2017): 981-996.
[25] Daabo, Ahmed M., et al. "Parametric study of efficient small-scale axial and radial turbines for solar powered Brayton cycle application." Energy Conversion and Management 128 (2016): 343-360.
[26] Guillaume, Ludovic, et al. "Performance of a radial-inflow turbine integrated in an ORC system and designed for a WHR on truck application: An experimental comparison between R245fa and R1233zd." Applied Energy(2016).
[27] Klein, SA Engineering equation solver. F-chart Software, Middleton, WI; 2013.
[28] ANSYS 15 CFX-Solver Theory Guide.
[29] Daabo, Ahmed M., Saad Mahmoud, and Raya K. Al-Dadah. "Development of Small-Scale Axial Turbine for solar powered Brayton Cycle." Students on Applied Engineering (ISCAE), International Conference for. IEEE, 2016.
[30] H. Riazi, N.A Ahmed, Effect of the ratio of specific heats on a small scale solar Brayton cycle. Procedia Engineering 49 (2012) 263-270.
[31] O. E. Balje, Turbomachines: A Guide to Design, Selection and Theory, JohnWiley & Sons, New York, NY, USA, 1981.
[32] Rohlik H. E., "Analytical determination of radial inflow turbine design geometry for maximum efficiency," Tech. Rep. TN D-4384, NASA,Washington, DC, USA, (1968).
[33] Wei, Chenyu, and Shusheng Zang. "Experimental investigation on the off-design performance of a small-sized humid air turbine cycle" Applied Thermal Engineering 51.1 (2013): 166-176.
[34] Rogers C., "Mainline Performance Prediction for Radial Inflow Turbine in Small High Pressure Ratio Turbine," VKI Lecture Series 1987-07, (1987).
[35] Whitfield A. and Baines N., "Design of Radial Turbomachines", JohnWiley & Sons, New York, NY, USA, (1990).
[36] Moustapha H., Zeleski M. F., Baines N. C., and D. Japikse, "Axial and Radial Turbines", Concepts NREC, White River Junction, Vt, USA, (2003).
[37] Aungier H., "Turbine Aerodynamics: Axial-Flow and Radial- Flow Turbine Design and Analysis", ASME Press, New York, NY, USA, (2006).
[38] Dixon, S.L. and Hall C., "Fluid mechanics and thermodynamics of turbomachinery". Butterworth- Heinemann, Oxford, UK (2013).
[39] Suhrmann, J.F., Peitsch, D., Gugau, M., Heuer, T., and Tomm, U., 2010, "Validation and development of loss models for small size radial turbines." Proceedings of ASME Turbo Expo 2010: Power for land, sea and Air GT 2010, Glasgow, UK, Paper No GT (2010)-22666.
[40] Glassman AJ., "Computer program for design and analysis of radial inflow turbines". NASA TN 8164; (1976).
[41] Churchill SW. "Friction-factor equation spans all fluid-flow regimes". Chem Eng (1977);84:91–2.
[42] ANSYS Inc., ANSYS TurboGrid user's guide. 2011.
[43] ANSYS Inc., ANSYS TurboSystem user's guide. 2011.
[44] Ennil, Ali Bahr. Optimization of small-scale axial turbine for distributed compressed air energy storage system. Diss. University of Birmingham, 2016.

[45] McLallin, K.L.; and Haas, J.E., "Experimental Performance and Analysis of 15.04-cm-tip-diameter, Radial-inflow Turbine with Work Factor of 1.126 and Thick Blading". NASA TP-1730, (1980).
[46] Spence, S. W. T. and Artt, D. W. "Experimental performance evaluation of a 99.0mm radial inflow nozzled turbine with different stator throat areas". Proc. Instn Mech. Engrs, Part A, Journal of Power and Energy, (1997), 211 (A6), 477–488.
[47] Spence, S. W. T. "An experimental assessment of incidence losses in a radial inflow turbine rotor". Department of Mechanical Engineering, The Queen's University of Belfast, 1997.
[48] Futral, S. M. and Wasserbauer, C. A. "Off-design performance prediction with experimental verification for a radial inflow turbine". NASA Technical Report TN D-2621, (1965).
[49] Lei FU, Zhen-ping FENG, Guo-jun LI, Qing-hua DENG, Yan SHI, Tie-yu GAO. "Experimental validation of an integrated optimization design of a radial turbine for micro gas turbines". Journal of Zhejiang University-SCIENCE A (Applied Physics & Engineering). ISSN 1673-565X, Feb. (2015).
[50] Y.K. Choo and K.C. Civinskas, "Three-dimensional inviscid analysis of radial turbine flow and a limited comparison with experimental data". ASME Winter Annual Meeting Miami, Florida, November 17-22, (1985).
[51] R. Dambach, H. P. Hodson and I. Huntsman. "An experimental study of tip clearance flow in a radial inflow turbine". Turbomachinery Committee Best Paper Award (1998).
[52] Meitner, Peter L., and Arthur J. Glassman. Off-Design Performance Loss Model for Radial Turbines with Pivoting, Variable-Area Stators. No. NASA-E-455. NATIONAL AERONAUTICS AND SPACE ADMINISTRATION CLEVELAND OH LEWIS RESEARCH CENTER, 1980.
[53] Lampart, Piotr. "Investigation of endwall flows and losses in axial turbines. Part I. Formation of endwall flows and losses." Journal of theoretical and applied mechanics 47.2 (2009): 321-342.
[54] Horlock, J. H. "Losses and efficiencies in axial-flow turbines." International Journal of Mechanical Sciences 2.1-2 (1960): 48-75.
[55] Wasserbauer, Charles A., and Arthur J. Glassman. "FORTRAN program for predicting off-design performance of radial-inflow turbines." (1975).

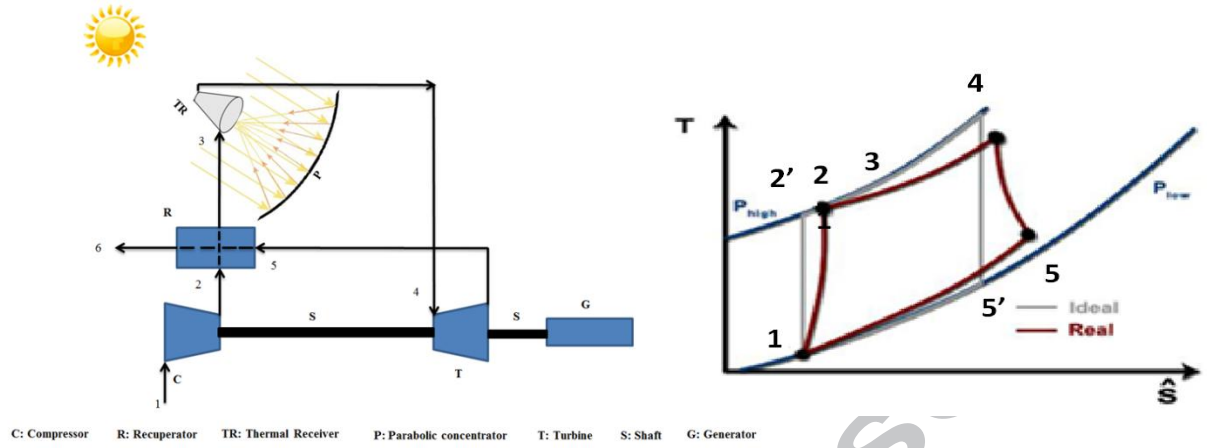

(A) **(B)**

Fig.1A: Schematic diagram of concentrated solar power with Brayton cycle system and the T-S diagram of the cycle in B.

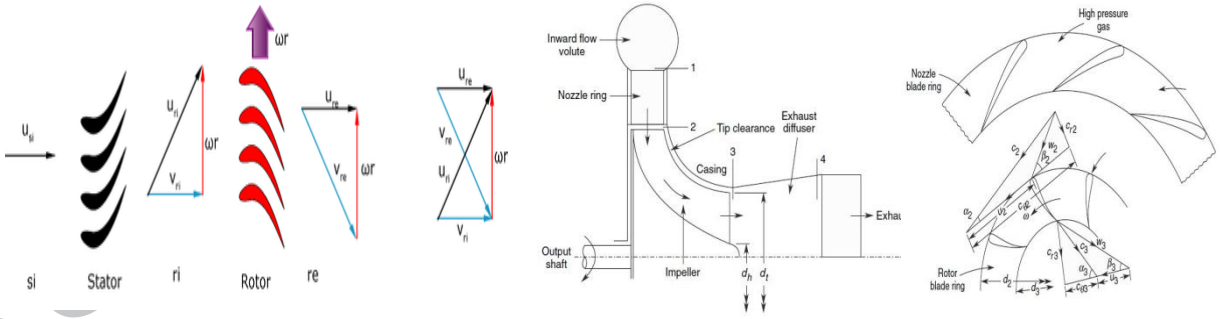

(A) **(B)**

Fig. 2: The mean line velocity triangle of; (A) axial turbine and (B) radial turbine [18].

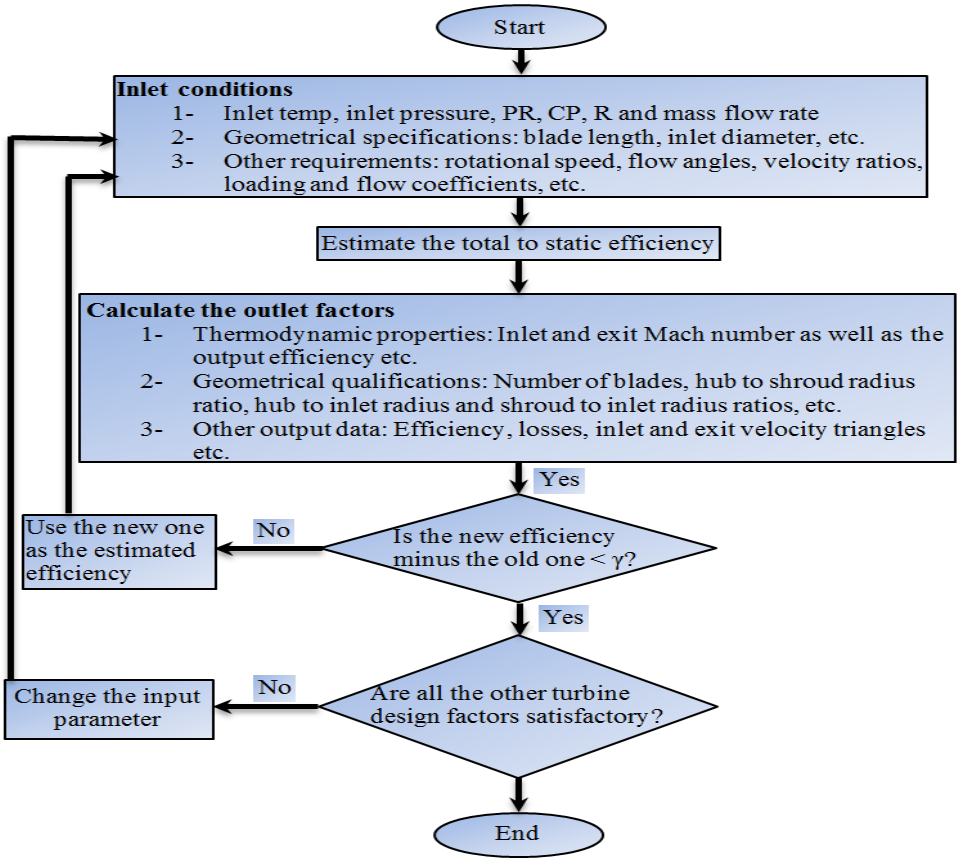

Fig. 3: Algorithm procedure used in the designed turbines.

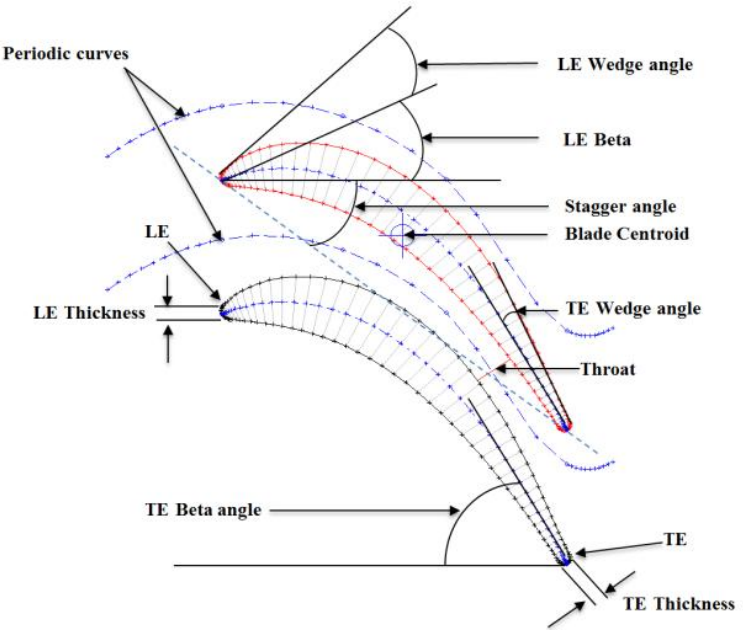

Fig. 4: The definition of the dimensions and the angles with Blade-to- Blade view.

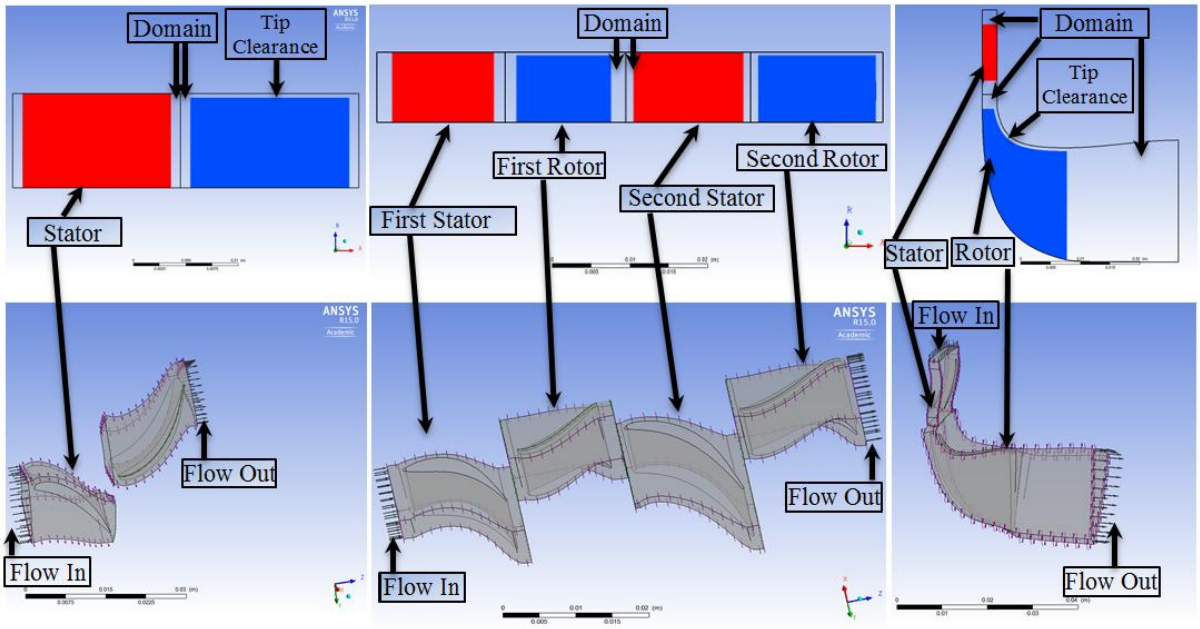

(A) **(B)** **(C)**

Fig. 5: 2D and 3D view for the blade of both the stator and rotor for the SSAT, DSAT and SSRT A, B and C respectively.

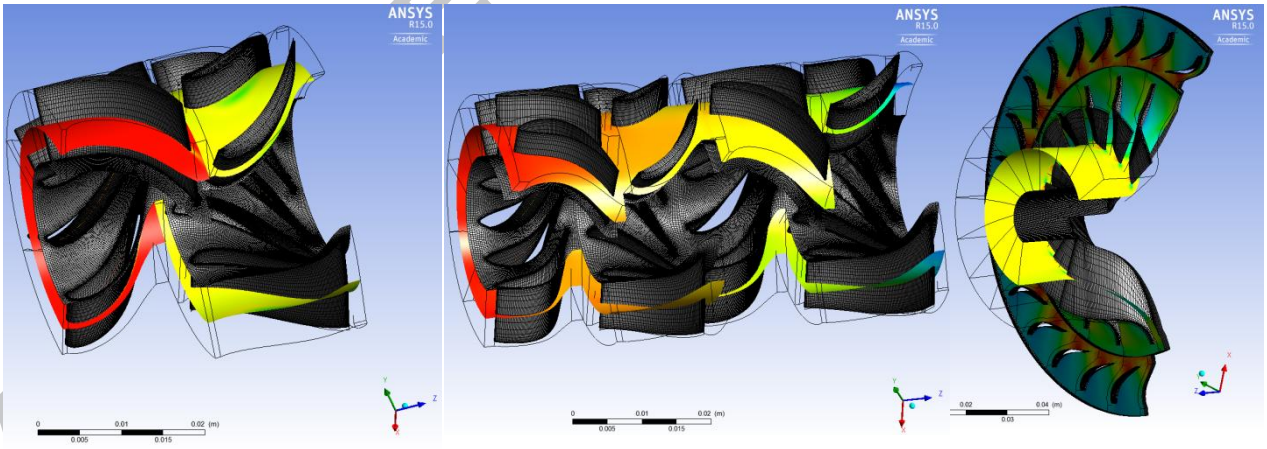

(A) **(B)** **(C)**

Fig. 6: 3D view for the all domains showing only the hub, the blades with their mesh lines of both the stator and rotor for the SSAT, DSAT and SSRT A, B and C respectively.

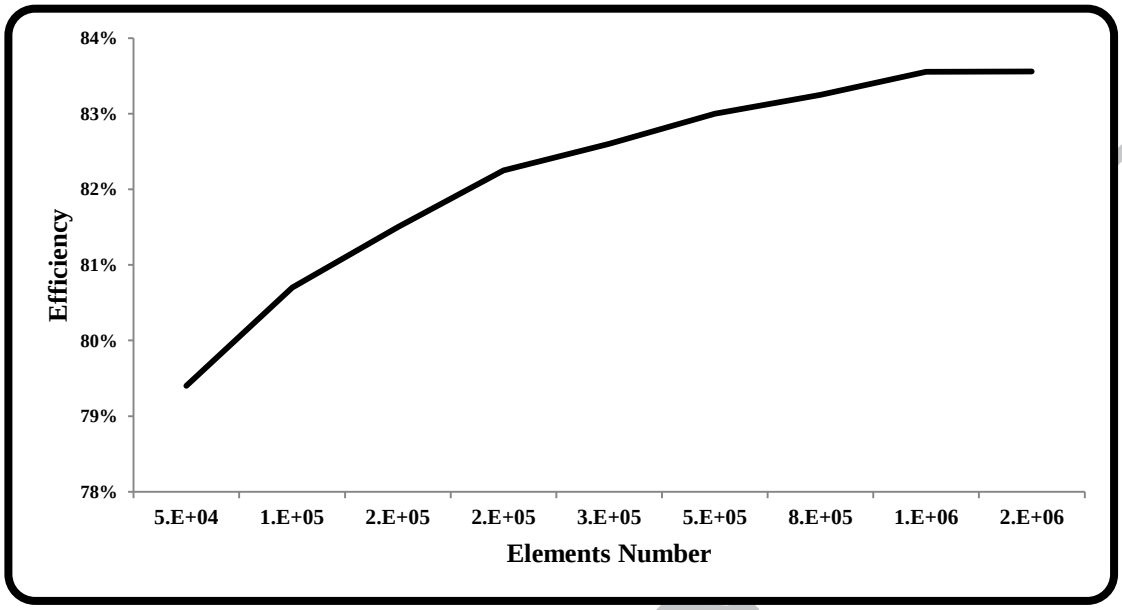

Fig. 7: Mesh sensitivity based on turbine efficiency.

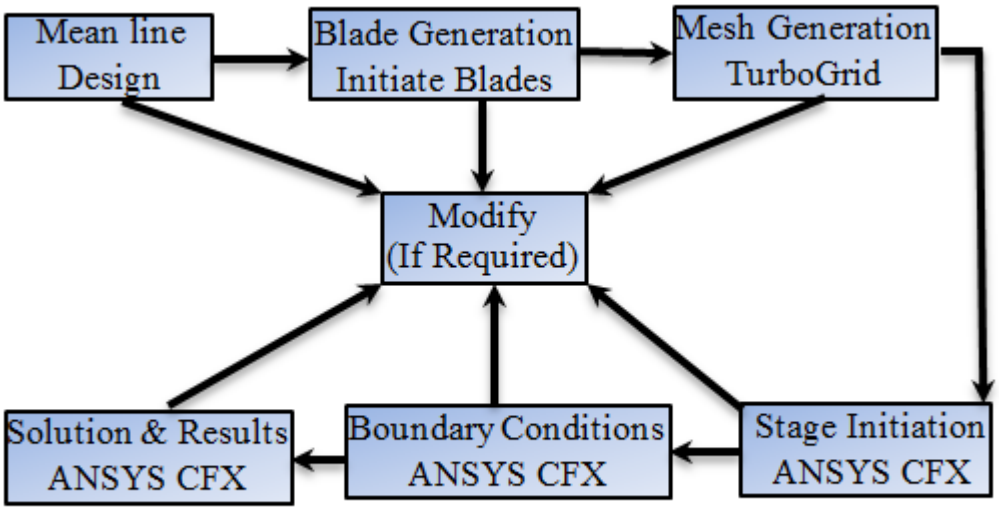

Fig. 8: CFD modelling procedure for the designed turbines.

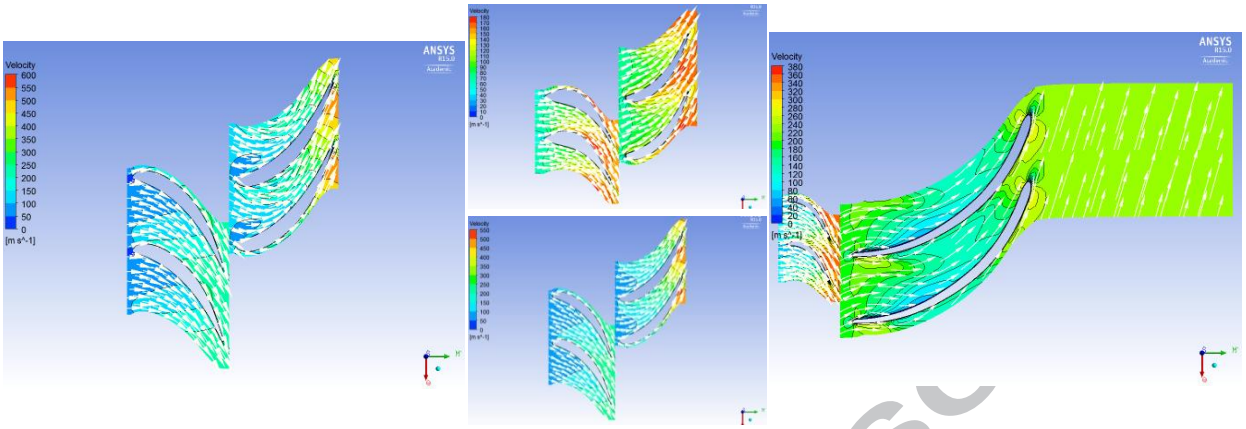

(A) **(B)** **(C)**

Fig. 9: Velocity distribution of stage, stator and rotor, for the SSAT, DSAT, 1st up, and SSRT A, B and C respectively.

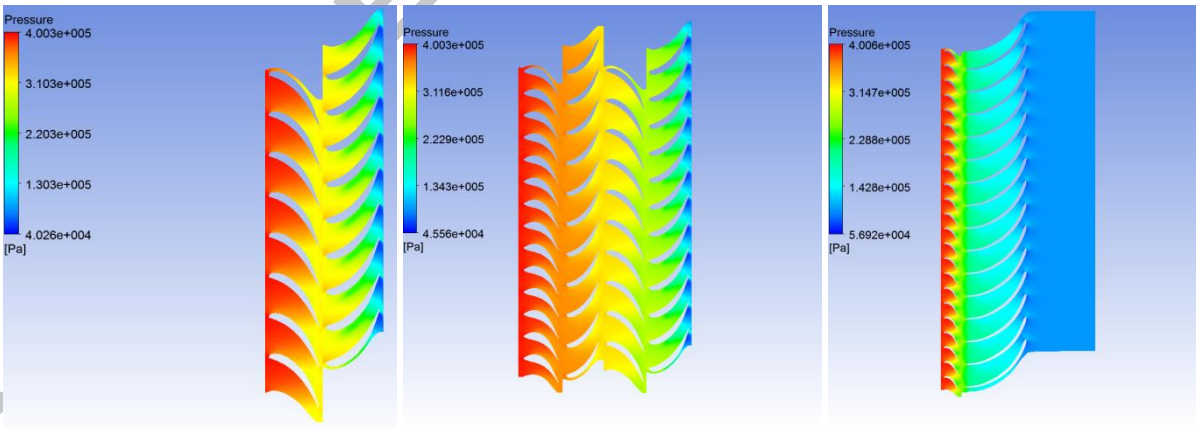

(A) **(B)** **(C)**

Fig. 10: Pressure distribution of stage, stator and rotor, for the SSAT, DSAT and SSRT A, B and C respectively.

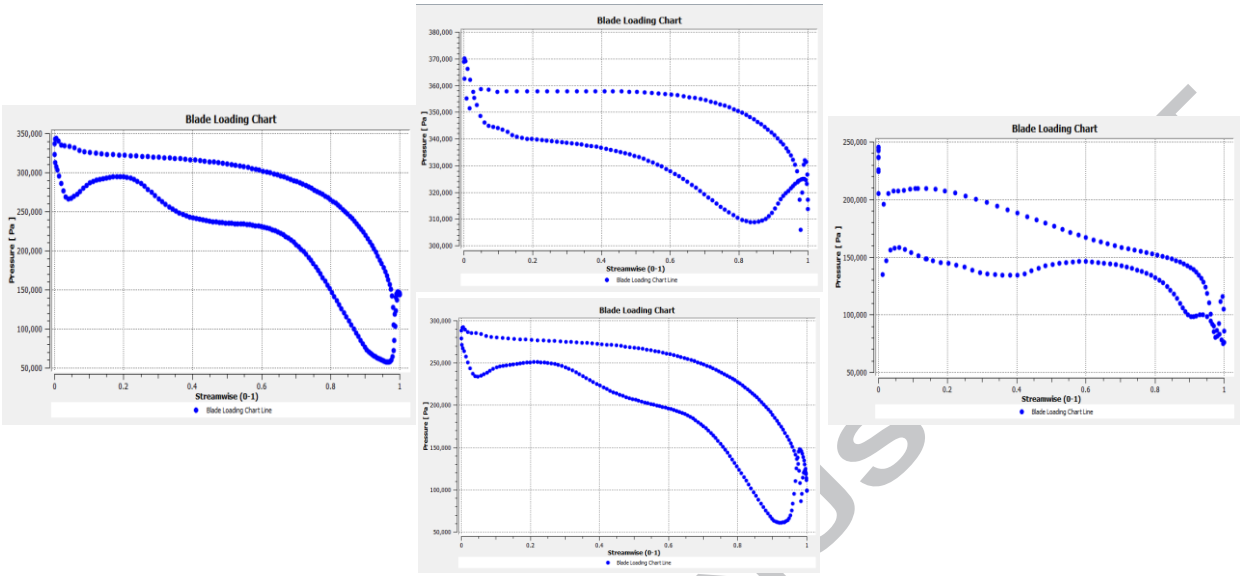

(A) **(B)** **(C)**

Fig. 11: Blade load distribution along the rotors for the SSAT, DSAT, 1st up, and SSRT A, B and C respectively.

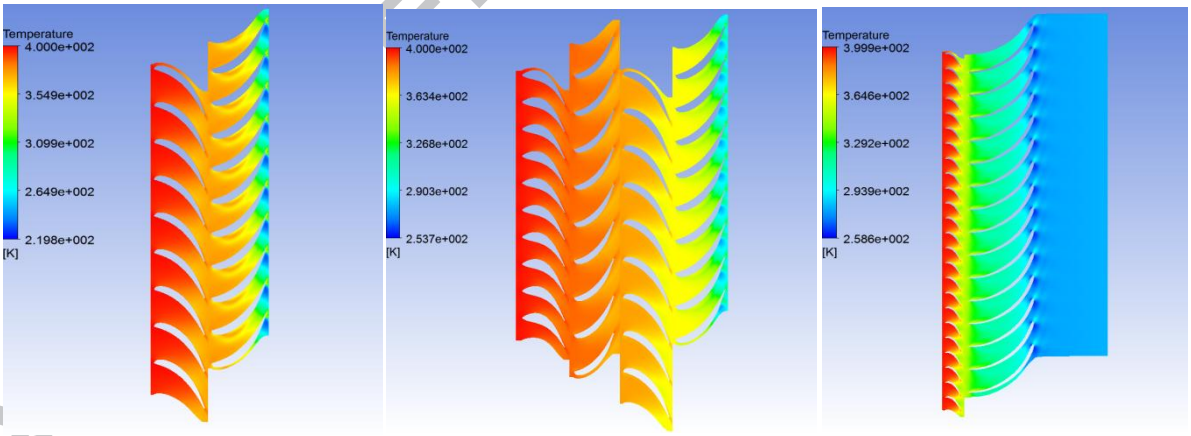

(A) **(B)** **(C)**

Fig. 12: Temperature distribution of stage, stator and rotor, for the SSAT, DSAT and SSRT A, B and C respectively.

(A)

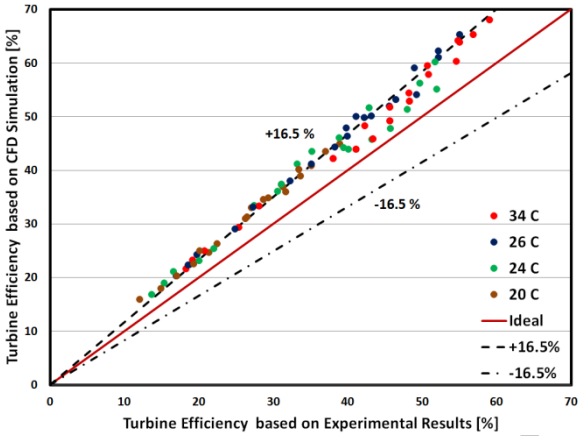

(B)

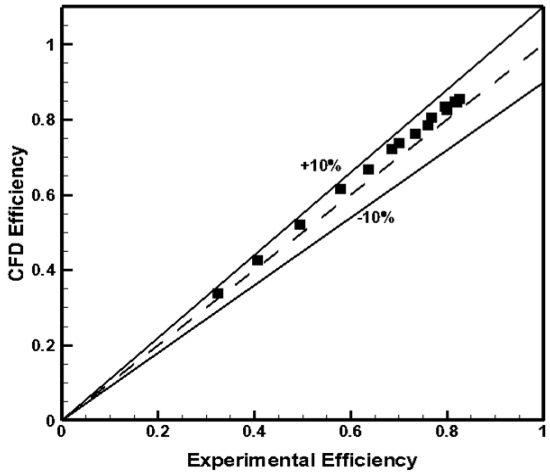

Fig. 13: The efficiency of the current work against two experimental works [44, 45].

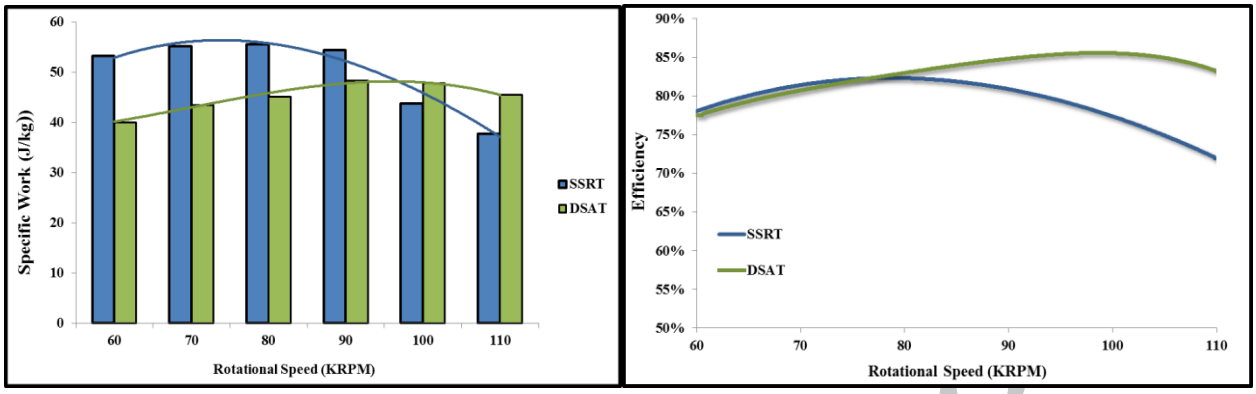

(A) (A)

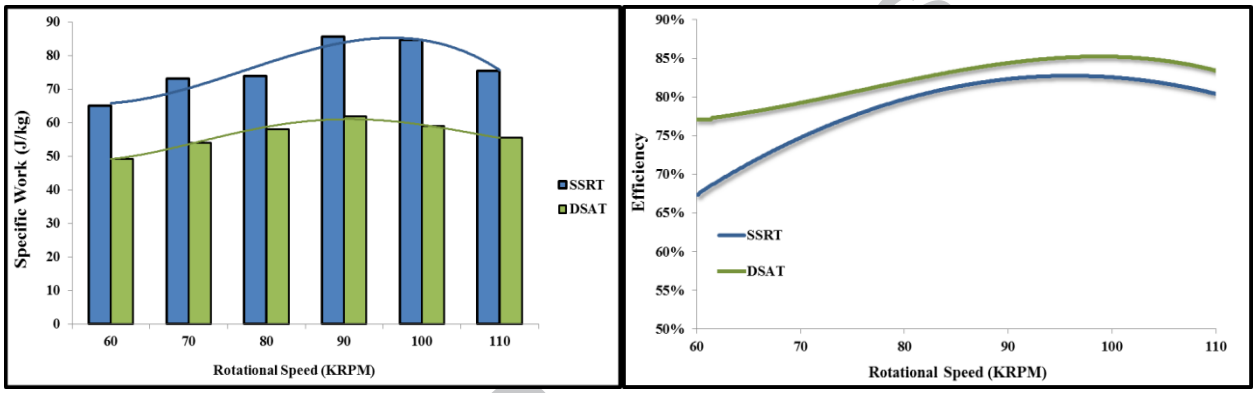

(B) (B)

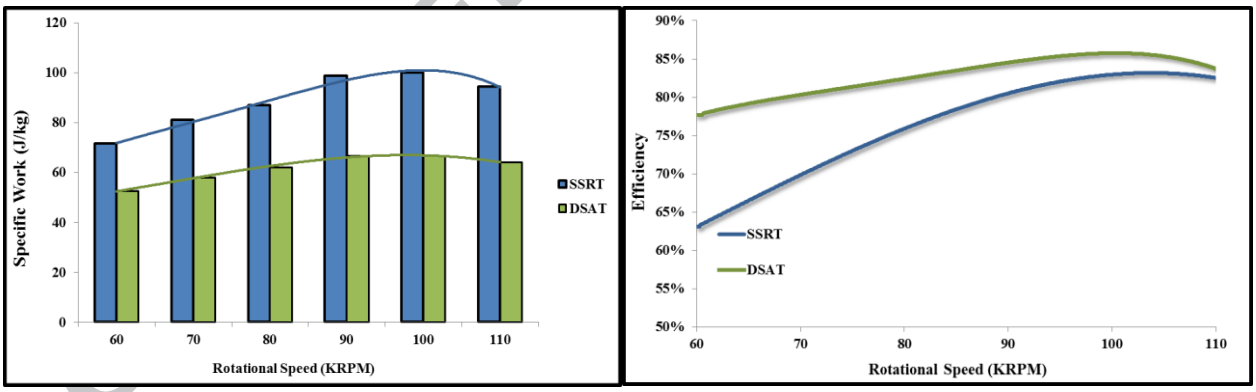

(C) (C)

Fig. 14: The turbine specific work and efficiency for the three turbines at different rotational speed, inlet temperature of 400 K and pressure ratio of; (A): 2, (B): 3 and (C): 4.

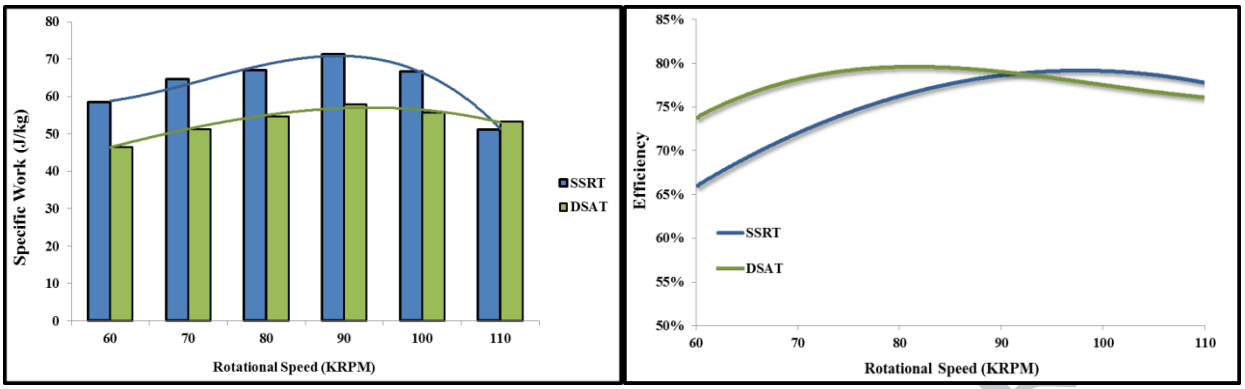

(A) **(A)**

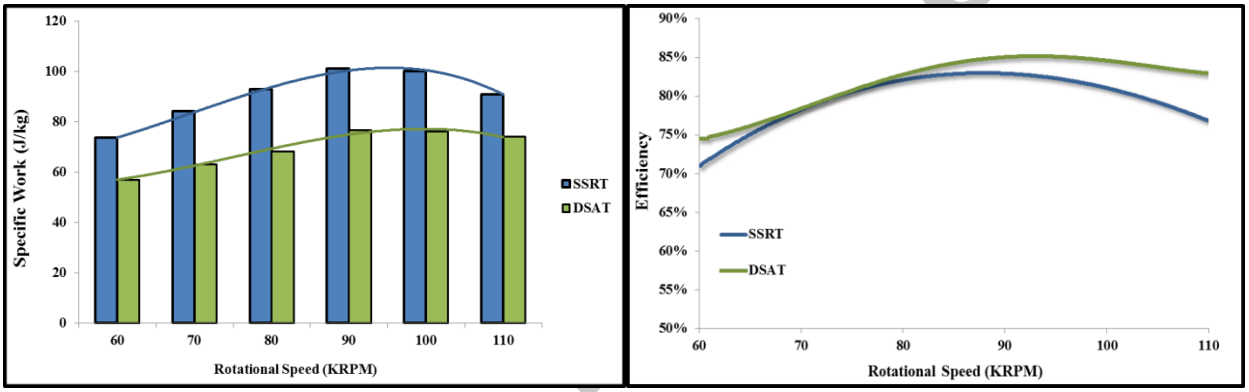

(B) **(B)**

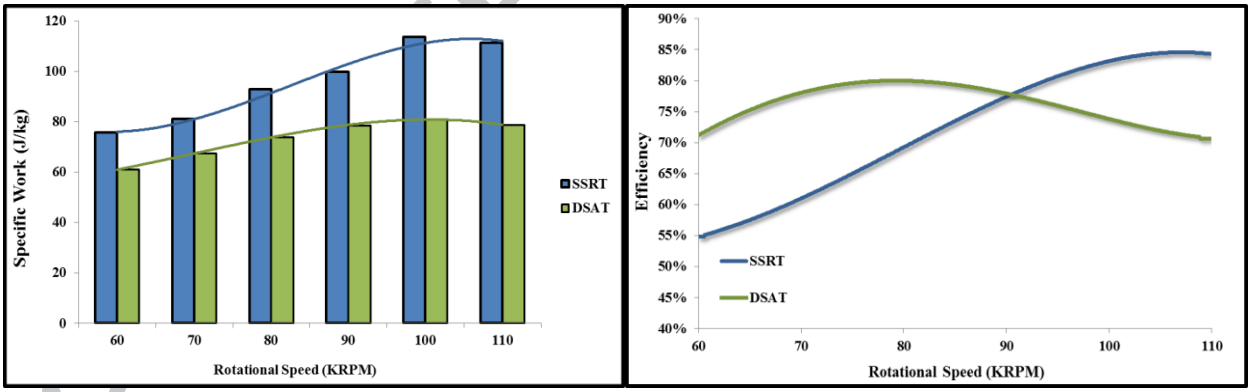

(C) **(C)**

Fig. 15: The turbine specific work and efficiency for the three turbines at different rotational speed, inlet temperature of 500 K and pressure ratio of; (A): 2, (B): 3 and (C): 4.

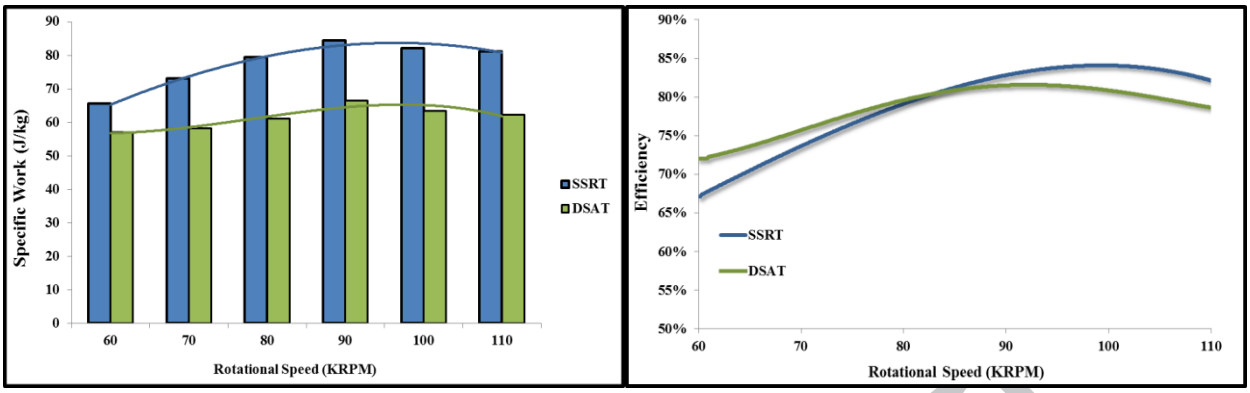

(A) **(A)**

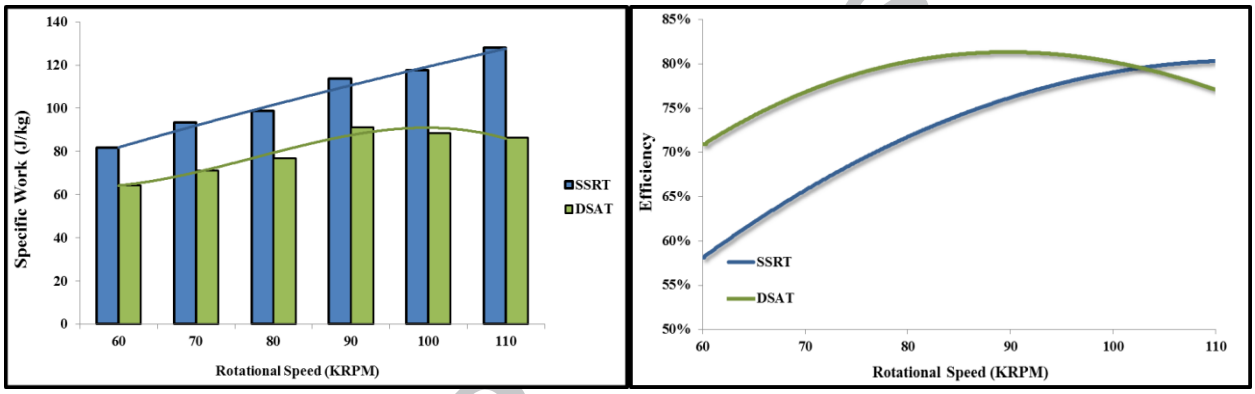

(B) **(B)**

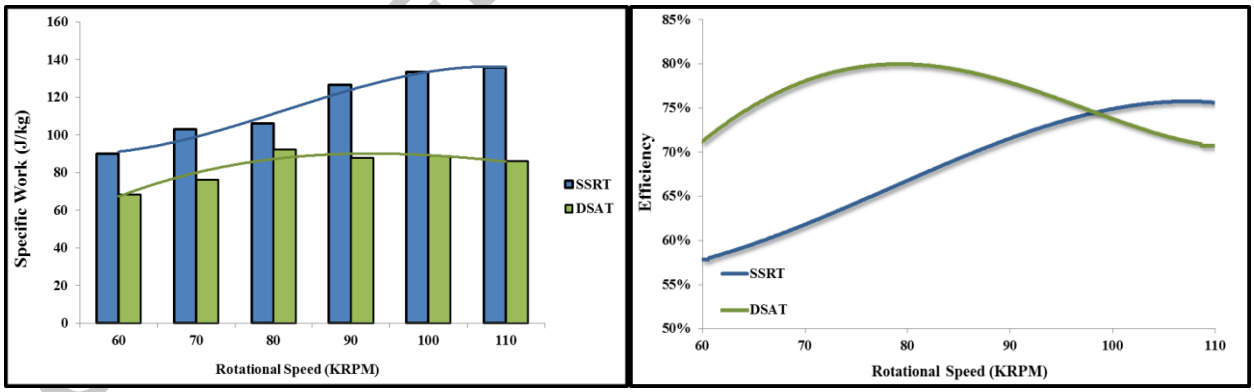

(C) **(C)**

Fig. 16: The turbine specific work and efficiency for the three turbines at different rotational speed, inlet temperature of 600 K and pressure ratio of; (A): 2, (B): 3 and (C): 4.

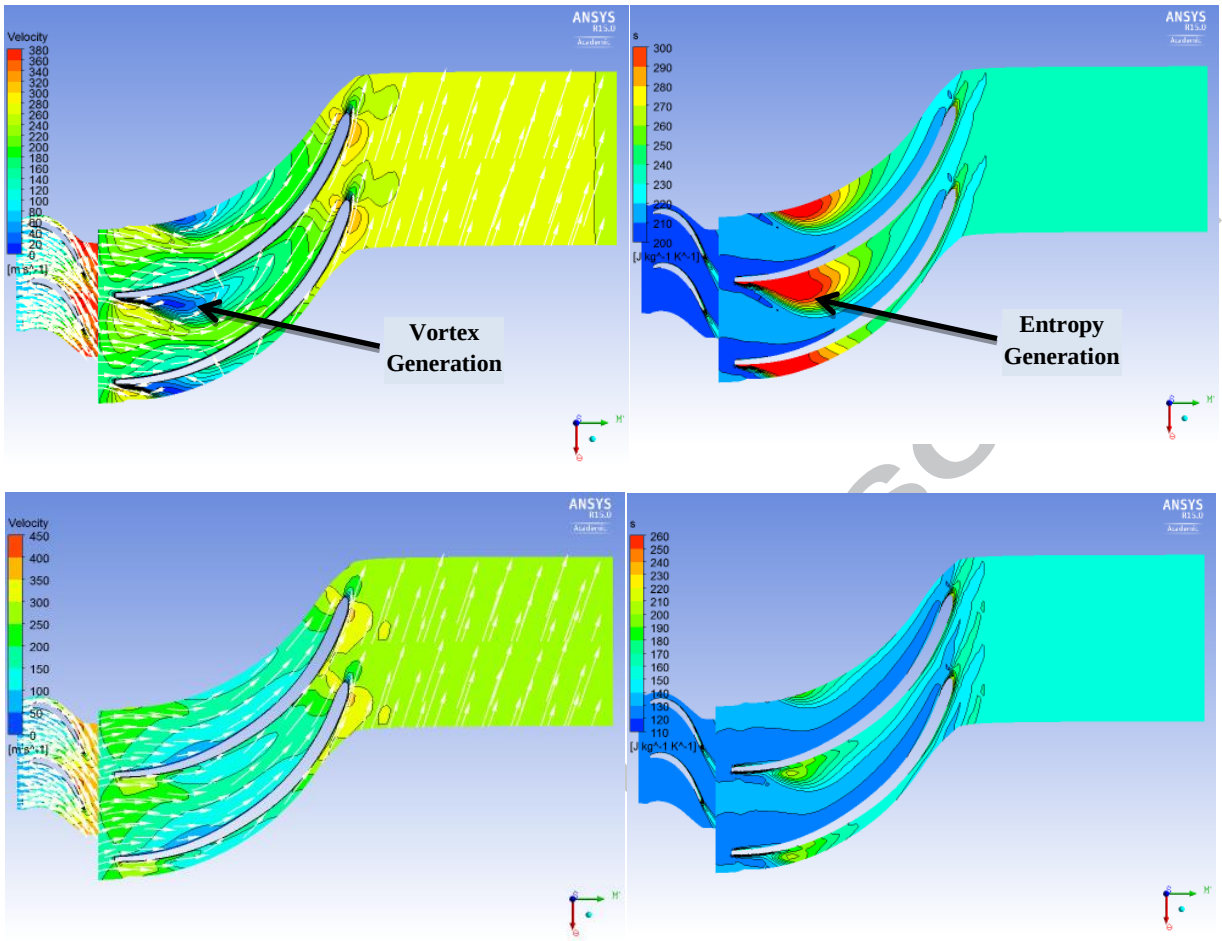

Fig. 17: Velocity distribution (left) and entropy generation for two different flow circumstances.

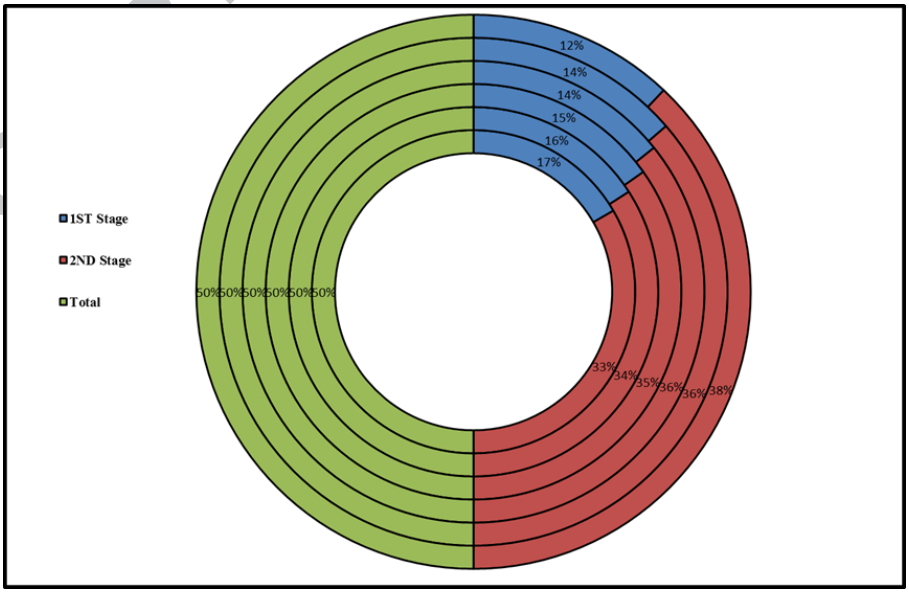

Fig. 18: The power output of each stage of the DSAT at different rotation speed, 60 KRPM matches the 12% and 110 KRPM matches the 17%.

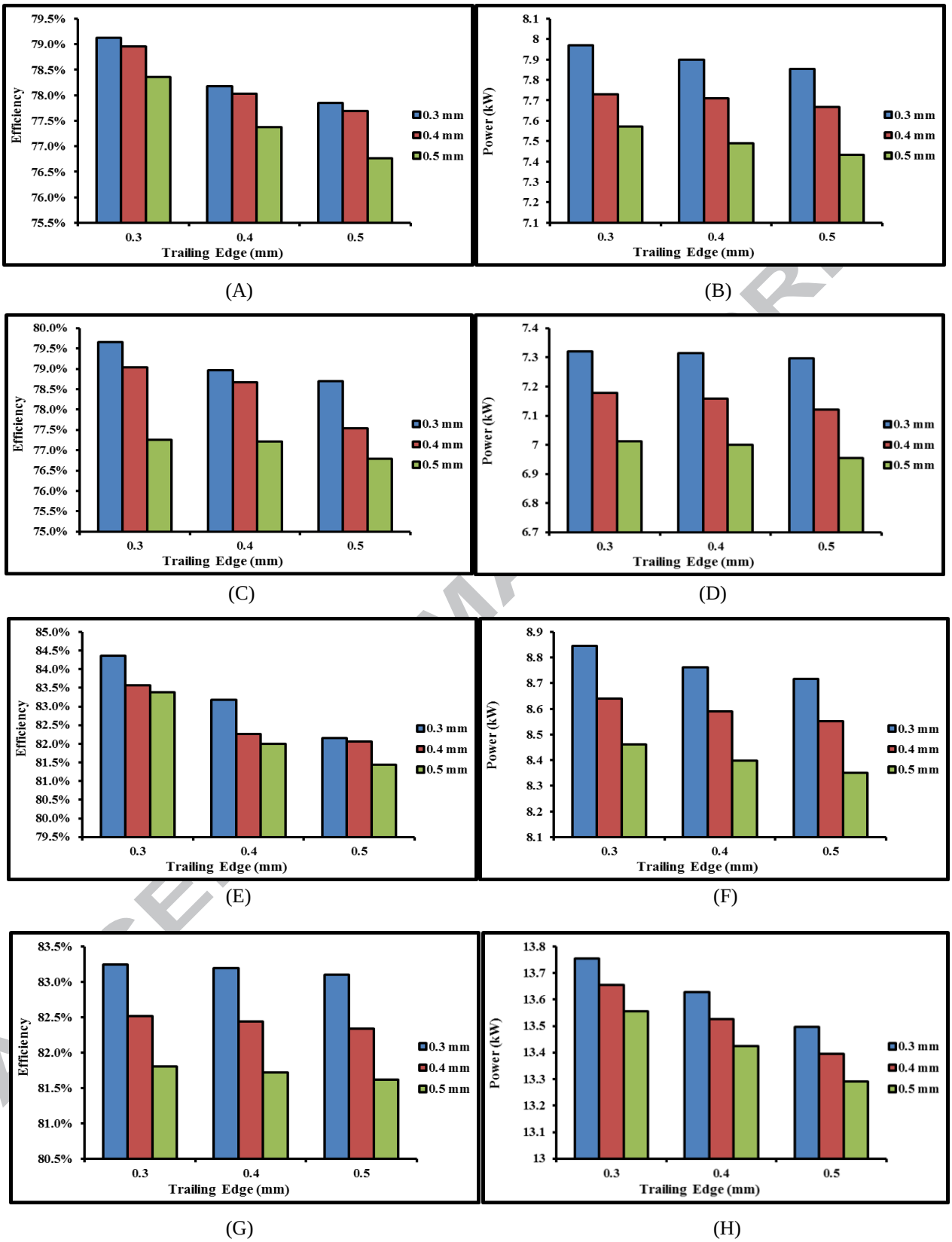

Fig. 19: The effect of stators' trailing edge values and tip clearance values on the efficiency, (A), and power output, (B), of the first stage of the DSAT, on the efficiency, (C), and power output, (D), of the second stage of the DSAT, the efficiency, (E), and power output, (F), of the DSAT and the efficiency, (G), and power output, (H), of the SSRT respectively at rotational speed of 90 KRPM, inlet temperature of 500 K and pressure ratio of 3.

(A)

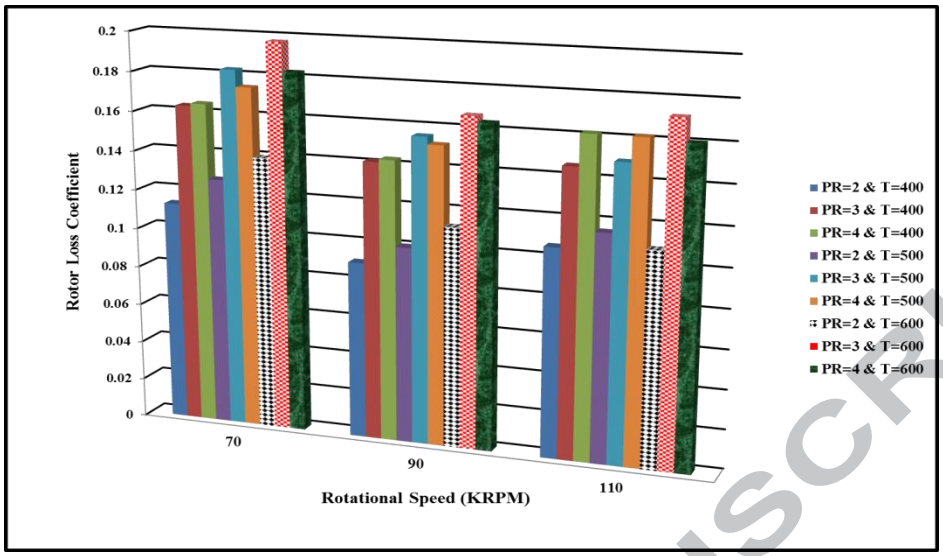

(B)

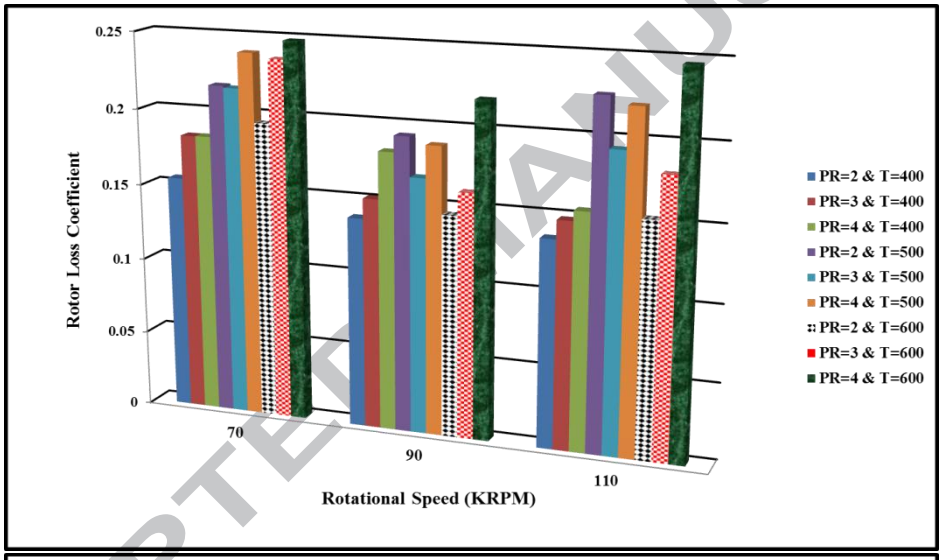

(C)

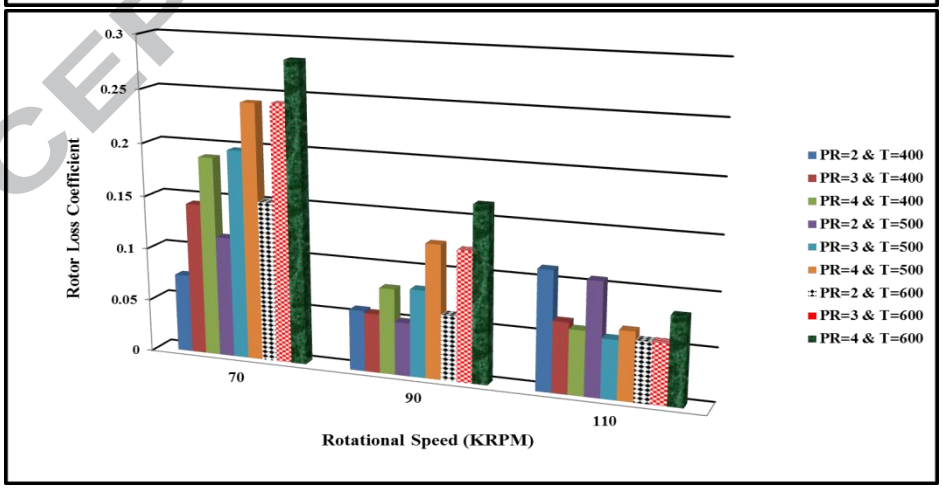

Fig. 20: Rotor total loss coefficient during the all studied boundary conditions for the SSAT, DSAT and SSRT A, B and C respectively.

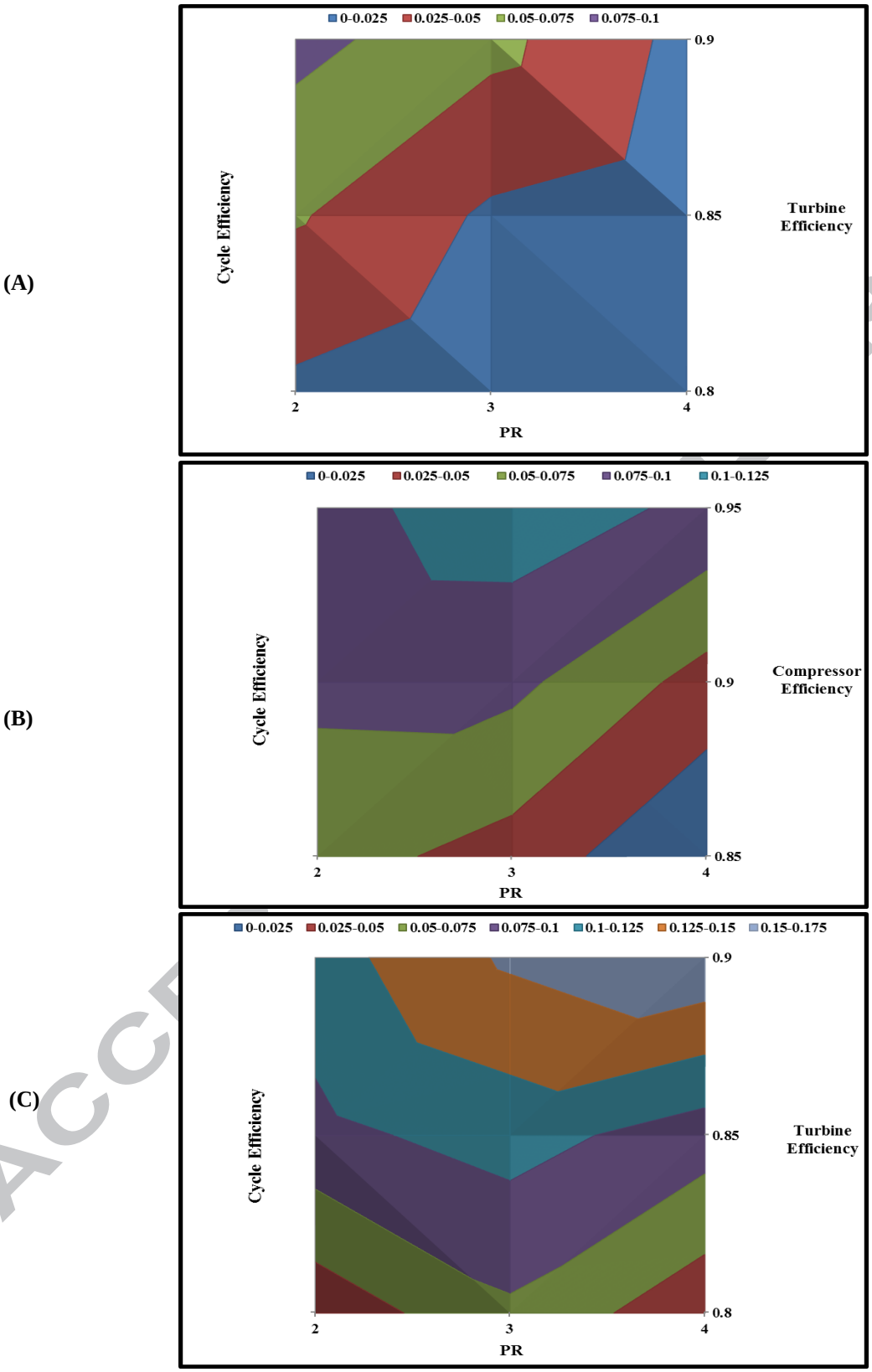

Fig. 21: The effect of the turbine (A&B) and compressor efficiency (C) on the overall cycle efficiency at various pressure ratio inlet temperature of: (A) 500 K, (B) 600 K and (C) 600 K.

Table2. Input parameter of the three configurations for the mean line design.

	Value			
	Axial		**Radial**	
Output power (Target)	5.0- 45	5.0- 45	5.0- 45	kW
Flow coefficient (Ψ)	0.8-1.4	0.4-1, 0.6-1.3	0.6-1.2	-
Hub/tip radius ratio (r_h/r_t)	0.52	0.52	0.3	-
Total PR	2-4	2-4	2-4	Bar
Reaction (R_n)	0.6	0.9, 1.6	0.7 -1.5	-
Rotational speed	60-110	60-110	60-110	1000*RPM
Total inlet temperature	400-600	400-600	400-600	K
Working fluids	air	air	air	-

Table3. The dimensions from the mean line design.

Parameter	**Value**			
	SSAT	**DSAT**	**SSRT**	
Hub diameter (D_h)	20	20	20	mm
Tip diameter (D_t)	38	38	-	mm
Rotor number of blade	9	8,9	11-19	-
Stator number of blade	8	11,8	22-30	-
Rotor Stagger angle	45	45, 45	39	Degree
Stator Stagger angle	45	35,45	41	Degree
Tip clearance	0.45	0.45, 45	0.45	mm
Tip Width	-	-	1.95	mm
Blade height (H)	15	15, 12	-	mm
Relative Inlet flow angle (β_2)	21	63, 66	10	Degree
Relative outlet flow angle (β_3)	-45	-63, -56	-79	Degree
Absolute inlet flow angle (α_1)	66	63, 66	0.0	Degree
Absolute outlet flow angle (α_2)	-43	3, -43	71	Degree

Graphical abstract

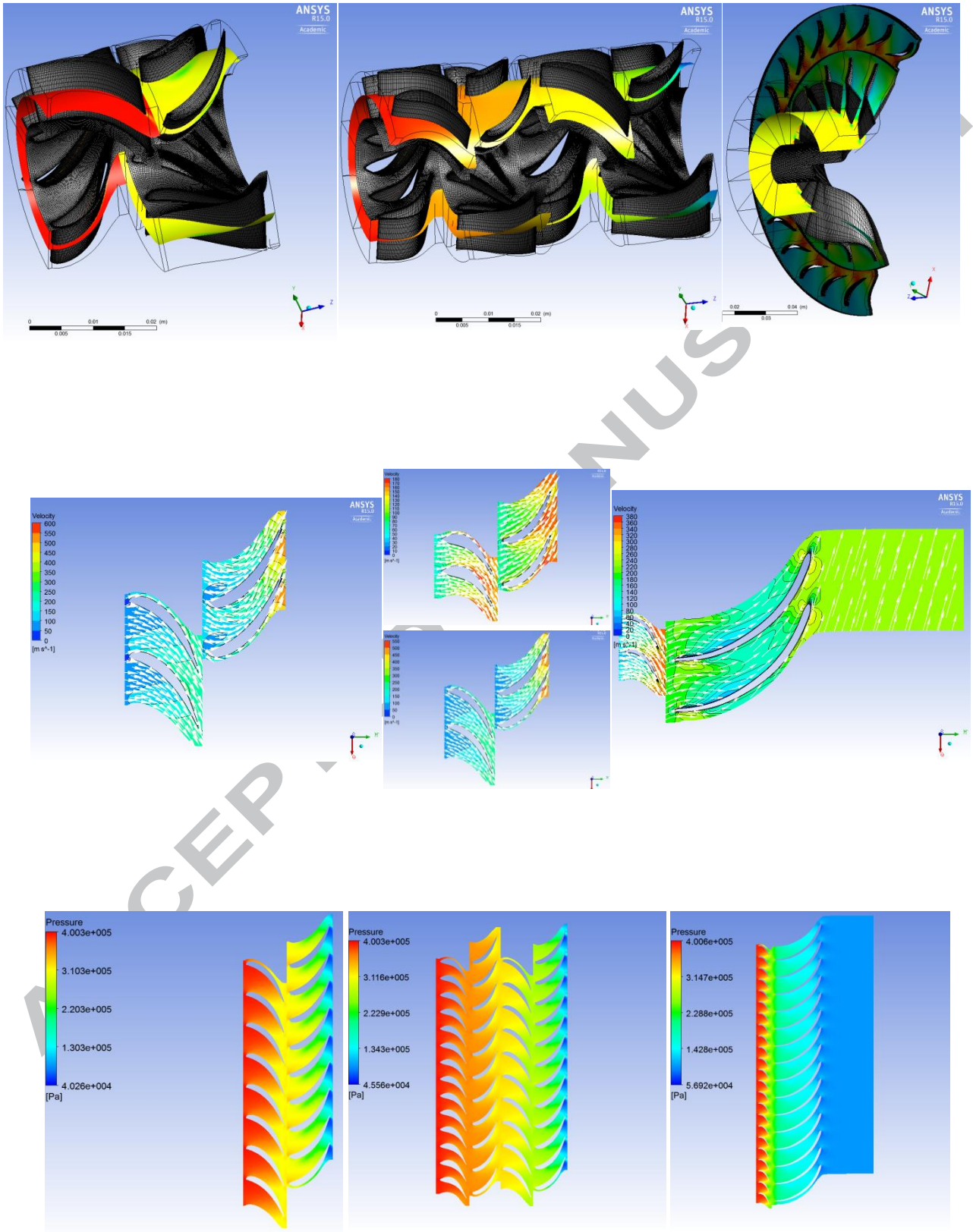

Highlights:

- 1D and 3D CFD analysis for compressed air turbines was carried out.
- Small scale single stage and dual stage axial turbine.
- Small scale single stage radial turbine.
- Loss assessment for the three configurations has been achieved.
- Enhancing their performance for solar powered Brayton cycle application.